Petermann Glacier on the Brink: Progress, Challenges and Insights

Dominik Fahrner[1], William T. Colgan[1], Joseph A. MacGregor[2], Peter Washam[3], Anja Løkkegaard[1], Shfaqat Abbas Khan[4]

[1] Geological Survey of Denmark and Greenland, Copenhagen, Denmark

[2] Cryospheric Sciences Laboratory, NASA Goddard Space Flight Center, Greenbelt, Maryland, United States of America

[3] Cornell University, Cornell Center for Astrophysics and Planetary Sciences, Ithaca, New York, United States of America

[4] DTU Space, The Technical University of Denmark, Kgs Lyngby, Denmark

Corresponding author: Dominik Fahrner (domfa@geus.dk)

Abstract

Petermann Glacier, the largest marine-terminating glacier in northern Greenland based on catchment area and ice discharge, plays a key role in regulating ice discharge from the Greenland Ice Sheet into the Arctic Ocean. With an upstream catchment connected to the ice sheet interior via a deep subglacial canyon, its future stability has major implications for sea level rise. In this review, we synthesize recent advances in understanding Petermann's dynamics across three critical interfaces: the ice–ocean , ice–atmosphere, and ice–bed boundaries. At the surface, observations show that reanalysis products underestimate air temperatures and melt, while regional climate models diverge significantly in their estimates of surface mass balance, underscoring the need for improved in situ data and models. At the ocean boundary, enhanced basal melting driven by both subglacial runoff and Atlantic water intrusions is identified as the dominant driver of recent mass loss of Petermann Glacier, with continued warming posing

a serious threat to the stability of the floating tongue. At the bed, new geophysical synthesis reveals complex geology, likely spatial variability in geothermal heat flux, and the influence of the megacanyon on seasonal hydrology and velocity fluctuations. Petermann's mass balance has been negative in recent decades without corresponding flow acceleration. However, the glacier has undergone significant calving events, and the current rifting that began in September 2025 highlights its vulnerability. This upcoming calving event underscores the timeliness of this review, as it will put Petermann Glacier's terminus at its most retreated position since records began in 1923. The anticipated retreat of the ice tongue also reduces buttressing and brings the terminus closer to the grounding zone, and modeling studies suggest that calving within 12 km of the grounding zone could potentially trigger dynamic retreat, accelerating ice discharge, and a doubling of flow speeds. We conclude that improved observations, sustained monitoring of oceanographic and atmospheric properties, and high-resolution modeling are critical to constraining projections of Petermann Glacier's future and its role in the stability of the Greenland Ice Sheet.

1. Historical Evolution

Petermann Glacier retreated from its largest extent in the Holocene ~7.5 ka BP from the outer sill into Petermann Fjord (*26*). Reconstructions and geophysical data suggest this retreat was followed by a complete collapse of the ice tongue ~6.8 ka BP, which is hypothesized to be due to Marine Ice Cliff Instability (*26*, *27*). Between 6.8 and 2.2 ka BP air temperatures were 0.8–2.9 K higher than pre-industrial times (*28*) and relatively mobile sea ice facilitated the increased transport of warmer Atlantic Water into Petermann Fjord, thus preventing the formation of an ice tongue (*26, Detlef et al., 2021*). Sediment records show that Petermann Glacier's ice tongue was reestablished ~2.2 ka BP, during long-term regional cooling, with the pre-2010 extent being reached between 0.4 and 0.9 ka BP when temperatures were coolest during the Holocene (*26*).

The existence of Petermann Fjord was reported during the U.S. Polaris expedition in 1871, but the existence of Petermann Glacier was not confirmed until 1875/76, when a British expedition suggested that a large glacier must feed into the fjord (*7*, *8*). During this expedition, Petermann Glacier's terminus was mapped at the entrance of Petermann Fjord and large fissures in the floating tongue were noted (Coppinger, 1877). In 1922, Lauge Koch observed the terminus had remained in the same location since the British Arctic Expedition (Koch, L, 1928), whereas in 1962 it had retreated by approximately 6 km (Davies and Kirnsley, 1962). While the naming of the glacier is not definitively traceable, it is commonly assumed that the glacier has been named during this expedition after German geographer August Petermann for his contribution to polar exploration (*8*). Petermann Glacier does not have a Greenlandic name (Bjork et al., 2015).

2. Recent Evolution

The Greenland Ice Sheet (GrIS) has been losing mass since the end of the Little Ice Age (~1900) and has experienced a sharp increase in mass loss since the mid to late 1990s, with marine-terminating glaciers now contributing 30–60% to the annual mass loss of the GrIS (*1*–*3*). Petermann Glacier is the largest glacier in northern Greenland, based on ice discharge and catchment area, with an ice volume equivalent to 0.38 m of global sea level (*4*) and a catchment that covers ~4% of the GrIS area (Fig. 1) (*2*, *5*, *6, 89, 90*). It is one of the few remaining marine-terminating glaciers in Greenland with a floating ice tongue, along with the North Greenland Ice Stream (NEGIS) and Ryder Glacier, which extends ~50 km from the grounding zone into Petermann Fjord.

Many glaciers in Greenland are grounded on bedrock at or near their marine terminus. The area where the ice transitions from resting on a grounded bed to floating on the ocean is referred to as the grounding line (*9*). In contrast to other marine-terminating glaciers in Greenland, Petermann Glacier is more analogous to Antarctic ice shelves, whereas the ice transitions from being in contact with bedrock to freely floating over several kilometers, due to its floating ice tongue (*10*). At Petermann Glacier, we refer to this transition zone as grounding zone. The extent of the grounding zone of Petermann Glacier is tidally modulated and can be up to 6.5 km in along-flow width (Fig. 1) (*4*). Remote sensing suggests that over the past two decades, this grounding zone has widened from 1.5 to 6.5 km in its center and retreated several kilometers (Fig. S1B) (*4*, *9*, *11*, *12*). This retreat began along its shear margins and then translated to just west of the glacier centerline. Enhanced basal melting due to long-term ocean warming (*13*) has been implicated as the driver of this retreat (*9*). However, Petermann experiences large seasonal variations in ocean-driven melting due to subglacial runoff of summer surface meltwater across the grounding line (*14*). This process can enhance submarine or basal melting by entraining warmer ocean waters in a turbulent plume, thereby increasing heat flow towards the glacier front or floating tongue (e.g. Motyka et al., 2003, Slater and Straneo, 2022).

Between 2016 and 2022, the grounding zone retreat resulted in the formation of a grounding zone cavity that experiences comparatively higher basal melting with average melt rates of up to 60 ± 15 m yr^{-1}, as estimated with remote sensing, coincident with summer subglacial runoff (Fig. 1 D-F) (4,*15*, *16*).

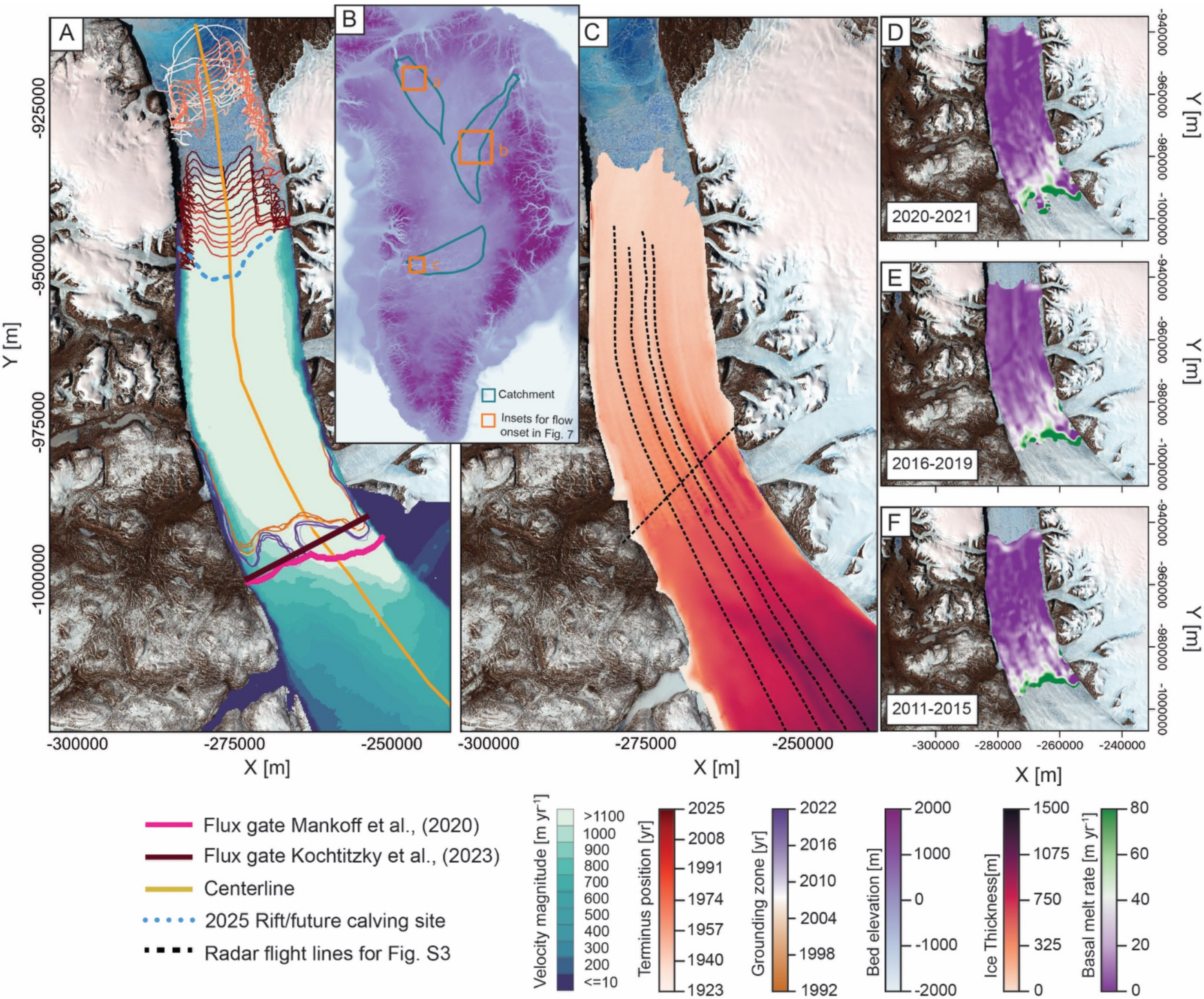

Figure 1 | Overview of Petermann Glacier

Overview of Petermann Glacier. ***A)*** *Terminus positions (17, 18) between 1923 and 2025 (manually delineated using GEEDiT) (19) colored by year (white to red) and grounding zones between 1992 and 2022 (4), also colored by year (orange to purple). The rift that initiated the ongoing calving event (delineated using Sentinel-1; Fig. S2) is shown as a light-blue dashed line and highlights that it will become Petermann Glacier's most retreated position since 1923 . The X and Y axes are polar stereographic coordinates (EPSG: 3413). Flux gates (20–22) are pink and brown, and the centerline is yellow. Basemap is a pan-sharpened Landsat-8 image from 17 June 2024 overlaid with MEaSUREs v5 mean annual ice surface speed (23).* ***B)*** *Location of Petermann Glacier, NEGIS and Sermeq Kujalleq (Jakobshavn Isbræ) catchments (teal; 64) with insets for Fig. 3 shown in orange on top of bedrock topography from BedMachine v5*

(*24*, *25*). ***C)*** *Ice thickness from Bedmachine v5 (24, 25) with flight lines for Figure S3 shown in black. Basemap is a pan-sharpened Landsat-8 image from 17 June 2024.* ***D-F)*** *Recent basal melt rates from Ciraci et al., 2023 for 2020-2021, 2016-2019, and 2011-2015, respectively.*

Over most of its observed history, Petermann Glacier has been stable, with relatively little terminus retreat (*5, Coppinger, 1877, Koch 1928, Davies and Kirnsley, 1962*). However, in the last two decades, large calving events have shortened its tongue by ~40 km, reducing its area by ~40% (*29*, *30*). The calving events produced ice islands with areas between 30 and 300 km^2, which are relatively small compared to the tabular icebergs that calve off Antarctic ice shelves, but comparatively large for Greenlandic glaciers (Crawford et al., 2018). Over the past quarter century, such calving events have occurred every 5 to 10 years, with some resulting in temporary increases in ice flow speed of ~10%, which are smaller than the subglacial-discharge-driven seasonal variability of ~25% (*31*–*35*). Using the break-up of the Holocene as an analog, it has been suggested that the increasing air temperatures of the recent decades have already destabilized the floating tongue of Petermann Glacier and have increased the risk of its collapse (*26*). The latest Sentinel-1 synthetic aperture radar image from March 2026 shows that a new calving event is imminent, as two rifts are visible at ~12.8 km and 19 km from the terminus, with the latter appearing to have reached the full width of the glacier within the last 12 months (Fig. S2). Once this ice has calved off, Petermann Glacier's new terminus will be within 40 km of the grounding zone, its farthest upstream position observed since 1923 (Fig. 1). This places the ice tongue terminus closer to the region of increased buttressing hypothesized to be at ~12 km from the grounding zone, from which calving events could drive larger increases in flow speeds as suggested by a modeling study (*6*).

Increased calving is currently a minor contributing factor (~5%) to the recent mass loss of Petermann Glacier, compared to basal melting of the floating tongue (~75%) and surface melting (20%) (*36–38, Munchow et al.,2014,*). Since 1990, Petermann Glacier has experienced grounding line retreat and flow acceleration due to an increase in basal melting of the tongue. These melt rates have increased from approximately 24 ± 5 m yr^{-1} in the grounding zone in the 1990s to averages of 60 ± 15 m yr^{-1} in the center and >100 ± 15 m yr^{-1} at the eastern and western margin of the grounding zone in the early 2020s (*4*, *11*, *39*). Similar basal melt rates have been measured at the Northeast Greenland Ice Stream (NEGIS), with an average of 60 m yr^{-1} and maxima of >150 m yr^{-1} near the grounding zone (Zeising et al., 2024). Warm Atlantic waters are delivered into Petermann Fjord at depth along its southwestern side (*13*, *40*, *41*). These warm Atlantic waters occupy the fjord water column from the sill depth (380–500 m) to the seabed at ~1000 m, resulting in considerable oceanic heat available for ice melt (*13*, *40–42*). In contrast, at Ryder Glacier, which is to the northeast of Petermann Glacier, the sill provides greater protection from warm Atlantic waters than at Petermann Glacier, thereby reducing basal melt rates there and limiting retreat (Jakobsson et al., 2020).

A recent modeling study suggests that if the ocean warms by an additional 0.5–1 K – an increase that has been observed at NEGIS between the 1970s and 2010s– ice tongue break-up could be induced within the next 5 to 30 years, depending on the rate of warming (*43, Wekerle et al., 2024*). Crucially, this projection did not include the influence of atmospherically-driven surface melt on basal melting and therefore could represent a conservative timeline of collapse. This ice tongue breakup has the potential to drive large-scale retreat of Petermann Glacier, which has an upstream catchment that connects to the ice sheet interior via a ~750-km-long subglacial canyon that rests below sea level (*24*, *44*). In this way, Petermann Glacier's ice tongue collapse could result in dramatic thinning, and increases in ice discharge and velocity, , similar to the break-up of Sermeq Kujalleq's (Jakobshavn Isbræ) ice shelf in 1997 (*45*–*47*), with catchment-wide implications (section 5.4.1) (Felikson et al., 2017, 2021).

Atmospheric warming has also been shown to have a direct impact on basal melt rates, as greater subglacial runoff has been suggested to induce to faster basal melting of the floating tongue (*14*). Remote sensing has shown an expansion of surface melt area in northern Greenland between 1985–1992 and 2013–2020 (*48*). Increased summer meltwater runoff has been found to enhance buoyancy-driven circulation beneath the Petermann Ice Shelf, intensifying ocean-driven basal melting and producing melt rates approximately twice those observed during winter (Cai et al., 2017; Washam et al., 2019). . With expected earlier onsets of the melt season in the future (*50*), Petermann Glacier's seasonal acceleration will likely start sooner each year, and basal melting of the floating tongue will increase due to increasing subglacial runoff (*35*).

A previous study reviewed Petermann Glacier with an oceanographic focus and provided an excellent overview of the ice–ocean boundary (Münchow et al., 2016). Given new findings in the past decade, especially at the ice–bed and ice–atmosphere interfaces, and increasing risks to the future stability of Petermann Glacier by climate change, here we review recent advances in our understanding of the behaviour of Petermann Glacier. We structure this article into three sections that represent the dominant interfaces where various processes are influencing the glacier's mass balance: (3) ice–atmosphere boundary, (4) ice–ocean boundary, and (5) ice–bed boundary. In section 3 , we compare currently available observational data products with reanalysis data to assess the mass balance and behavior changes of Petermann Glacier over the past decades, identify gaps in our knowledge and highlight future data needs. In section 4 , we discuss recent findings concerning ocean heat delivery, submarine melting and long-term oceanographic trends. In section 5 , we discuss Petermann Glacier's underlying geology, geothermal heat flow and subglacial hydrology, and their influence on ice flow and basal melting. Finally, we provide an outlook on how recent changes at Petermann Glacier might impact its future and the stability of its floating tongue, and provide recommendations for future research efforts

3. Ice–Atmosphere Boundary

For the ice–atmosphere boundary, we focus on air temperature, surface mass balance, and ice velocity as the key observable parameters influencing the recent evolution of Petermann Glacier. By comparing different data products, namely 1) reanalysis and observational air temperature data, 2) three different surface mass balance products extracted from regional climate models (RCMs), and 3) two different ice velocity products, we aim to assess the current state of Petermann Glacier while also highlighting potential caveats in their interpretation and needs for future improvements therein.

3.1 Atmospheric Conditions

Directly observed air temperatures are only available within the catchment of Petermann Glacier from two GC-NET weather stations (*51*, *52*) and one automated weather station (PG16) established by the University of Delaware (*14*). The "Petermann Glacier" GC-NET weather station was located just upstream of the grounding zone during 2002–2006 at an elevation of 37 m, while the "Petermann ELA" GC-NET station has been located at the historical equilibrium line altitude (944 m) since 2003. The automatic weather station "PG16" was established 16 km from the grounding zone in August 2015 and provides complete data for 2017 (*14*). Off the ice, there is also a Danish Meteorological Institute (DMI) weather station in Hall Land, ~110 km from the floating tongue at an elevation of 105 m (*53*). Given the significant distance of both the DMI and "Petermann ELA" stations to the Petermann Glacier proper, we omit those stations to prevent skewing the analysis towards potentially colder temperatures. Observational data is therefore only available for 2002–2006 (GC-NET), and 2017 (PG16). The observed air temperatures are compared to reanalysis data from ERA5 (*54*), MAR 3.14 (Tedesco and Fettweis, 2020) and RACMO2.3 (*55*). The ERA5 reanalysis data provide air temperatures at a height of 2 m above surface, with a spatial resolution of 0.25° × 0.25° (~31 km; Hersbach et al., 2020), whereas RACMO2.3 and MAR 3.14 have a resolution of 0.1° × 0.1° (~11 km; 55, Tedesco and Fettweis, 2020; Noël et al., 2018). To correct for the elevation difference between GC-NET station and ERA5 grid cells, we calculate a minimum and maximum correction factor using lapse rates of 4.5 K km^{-1} and 7 K km^{-1} (Noel et al., Fettweis et al.,Dutra et al.,). For simplicity, we use a mean lapse rate of 5.5 K km^{-1} (*56*) for the comparison of ERA5 data to observational data.

The comparison of air temperatures from weather stations, ERA5, MAR 3.14 and RACMO2.3 for the period 2002 to 2005 and for 2017 shows that the reanalysis data can generally capture the seasonal variability in the observational data (Fig. 2A). Given that surface meltwater can be an important driver for ice dynamics at Petermann Glacier, we focus our specific analysis on the summer melt season, between June and September of each year (*14*). During the investigated melt seasons (Fig. 2), GC-Net data shows positive degree days for 285 out of 364 days (78.3%), compared to 68 (18.6%) for ERA5, 266 (72.9%) for RACMO2.3, and 306 (84.1%) for MAR 3.14 (Figure S3). Similarly, PG16 shows 54 out of 88 total days (61.4%) being above 0°C compared to 15 days for ERA5 (17.1%), and 47 (53.4%) for RACMO2.3 (Figure S3). Only 80 days overlapped between MAR 3.14 and PG 16 data, with 51 days (66.3%) being above 0°C for PG16, and 66 (88.7%) for MAR 3.14 (Figure S3). Assuming a degree-day-factor between 5 and 9 mm d^{-1} $°C^{-1}$ (*57*), this would equal to a maximum total surface melt of ~554 cm (minimum: 307 cm) for GC-Net, ~263 cm (146 cm) for ERA5, 450 cm (250 cm) for RACMO2.3 (*58*), and ~664 cm (369 cm) for MAR 3.14 temperatures. For the 2017 melt season, this would equal to maximum surface melt at PG16 of 84.7 cm (minimum: 47 cm), with ERA5, RACMO2.3, and MAR 3.14 indicating 12.1 cm (6.7 cm) , 71 cm (39 cm), and 168 cm (93 cm), respectively.

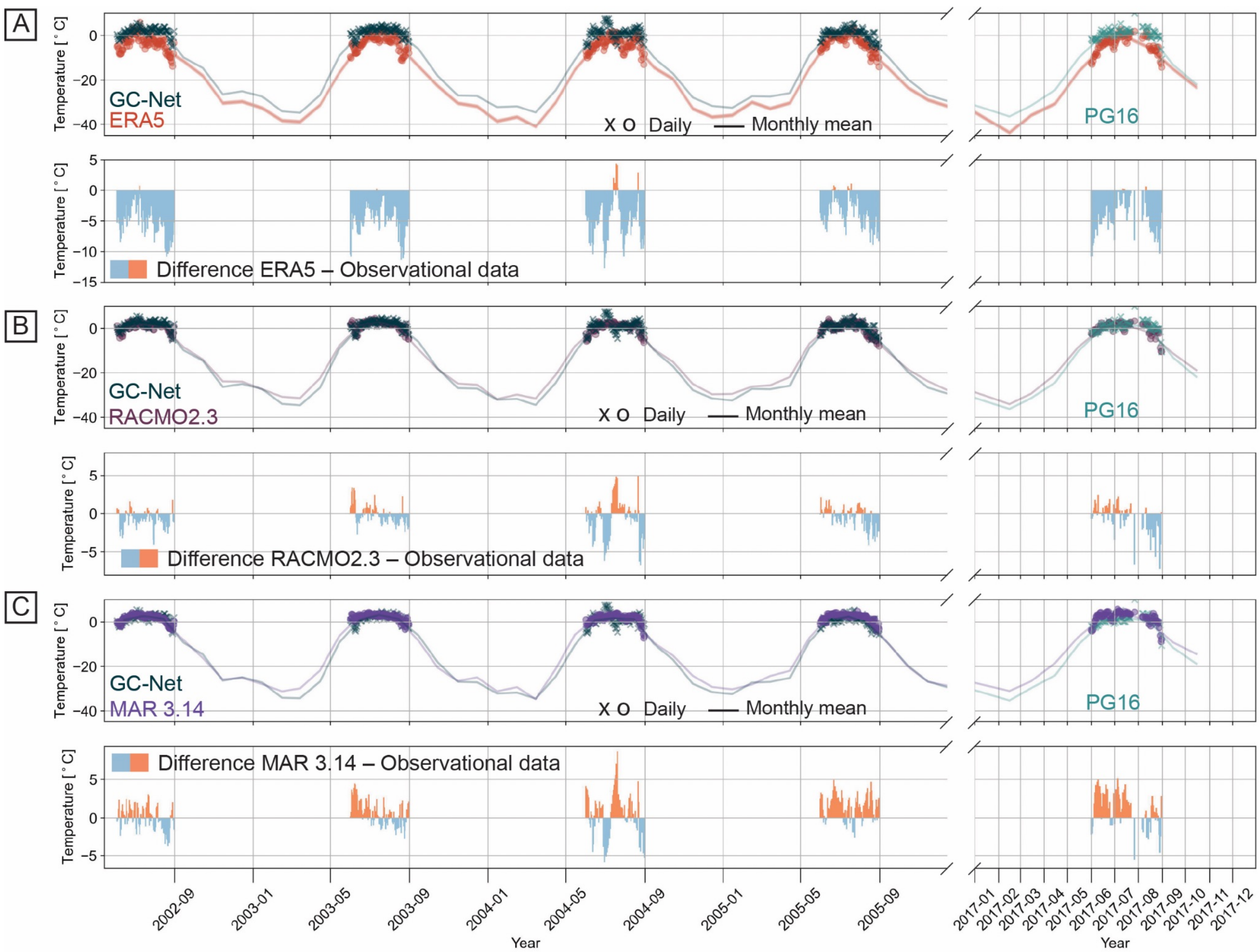

Figure 2 | Air temperature comparison for Petermann Glacier

*Comparison of air temperature data for **A)** Monthly mean air temperature data from GC-NET automated weather stations (51, 59) located at Petermann Glacier (dark green), monthly mean air temperature data from ERA5 (orange) (54), and monthly mean air temperature data from PG16 automated weather station (turquoise) (14). Daily values during the melt season (June-September) are shown for GC-NET (green x), ERA5 (red circle), and PG16 (turquoise x) c . For location of ERA5 grid cell and AWS locations see Figure S2. Below is the difference between daily ERA5 and observed air temperature data during the melt season (red=ERA5 temperature > observed temperature; blue=ERA5 temperature < observed temperature). **B)** Same as A) for RACMO2.3 reanalysis data (55). C) Same as A) for MAR 3.14 reanalysis data (Tedesco and Fettweis, 2020).*

This analysis shows that the bias towards colder air temperatures of ERA5 data has significant implications for estimating surface melting in the catchment of Petermann Glacier. Simply put, Petermann Glacier is likely experiencing more surface melt than suggested by ERA5, which should be taken into consideration when using that reanalysis to force the spin-up of ice flow models of Petermann Glacier. As highlighted below (Section 3.2), ERA5 reanalysis data features prominently in the current generation of RCMs simulating Greenland Ice Sheet surface mass balance. While RACMO has a significantly smaller bias towards colder temperatures than ERA5, it still underestimates the number of positive degree days and consequently the amount of surface melting. On the other hand, MAR 3.14 shows a significant overestimation of positive degree days and surface melting, which should be taken into account when using this data. This comparison shows that the choice of reanalysis product is significant for investigations of surface processes. It further stresses that in-situ observational data is needed to validate reanalysis products, and to accurately determine surface melting at Petermann Glacier.

3.2 Supraglacial hydrology

Previous studies have shown that supraglacial lakes (SGL) form across the grounding zone and the floating tongue annually, starting in early June with the onset of surface melting (Macdonald et al., 2018, Zhu et al., 2023). Subsequently, SGLs increase rapidly in number, volume and area, before declining in July despite air temperatures often persisting above 0°C (Macdonald et al., 2018). A narrow channel in the center of the floating tongue, which has been identified as an area of thinner ice compared to the sides of the floating tongue, turns into a river coinciding with the onset of SGL development (Münchow et al., 2014, Macdonald et al., 2018). The development of SGLs has been associated with Antarctic ice shelf instability and break-up as has been observed on the Larsen B ice shelf in March 2002, for which SGLs covered up to 5.3% of its surface area prior to its breakup (Banwell et al., 2012, Macdonald et al., 2018). In comparison, during the 2014–2016 melt seasons, Petermann Glacier's floating tongue SGL coverage reached a maximum of 2.8% (Macdonald et al., 2018). While future increases in air temperatures could increase SGL development and thus instability of the floating tongue, the decrease in SGL volume despite positive air temperatures suggests that meltwater is drained somewhat efficiently, thereby limiting this destabilizing factor (Macdonald et al., 2018).

3.3 Ice Discharge

We review the ice discharge (D) as assessed for Petermann Glacier by previous monthly (*20*, *21*), annual (*2*, *55*) and decadal studies (*22*). Table S1 provides an overview of the differences in grounding line, or flux gate, assumption (Fig. 1), input datasets, and temporal resolution between the three data products. We note that the annual (*2*, *55*) and decadal datasets (*22*) correct for mass loss downstream of the flux gate using surface mass balance data, whereas the monthly dataset (*20*, *21*) does not.

This comparison of ice discharge products shows that a slight increase in discharge since the 1980s is captured in all products (Fig. 3A). While this pattern is supported when comparing decadal means, we find a significant difference in the magnitude of change between multi-decadal trends (Table S2). The annual (*2*, *55*) and decadal data (*20*, *21*) suggests an increase in ice discharge of 6% (0.7 Gt yr^{-1}) and 1% (0.1 Gt yr^{-1}) from 1990–2000 to 2000–2017, respectively (Table S2). Conversely, the monthly data (*20*, *21*) shows a 4% (–0.5 Gt yr^{-1}) decrease when comparing the same time periods (Table S2). As shown in Fig. 3A, seasonal variability can influence ice velocities, and thus ice discharge, by up to ~25%. This seasonality means that data products that capture the full seasonal velocity cycle yield a more accurate annual discharge than those that do not. Based on these results, we suggest that seasonal ice discharge products with resolutions no coarser than monthly (*20*, *21*) are preferred not only when assessing seasonal ice dynamics but also when investigating multi-decadal trends.

3.4 Surface mass balance

Despite the Petermann Glacier catchment encompassing 4% of the ice sheet's area, the only surface mass balance (SMB) measurements presently available are four years of in-situ SMB measurements from the "Petermann Glacier" weather station (*60*). Therefore, rather than comparing observed and modelled SMB, we instead perform an intercomparison of the SMB assessed by different models for the entire catchment of Petermann Glacier between 1980–2020. For this intercomparison, SMB is taken from ERA-Interim forced 5-km monthly HIRHAM5 data (*61*, *62*), ERA5 forced 1-km monthly MAR v3.14 data (*63*), and ERA-40/ERA-Interim forced 5-km RACMO2.3 data downscaled to 1 km (*2*, *55*). The different climate reanalysis datasets used to force the regional climate models have different spatio-temporal resolutions, with ERA-40 being the coarsest (~1°, 6-hourly), followed by ERA-Interim (0.75°, 6-hourly) and ERA5 (0.25°, hourly). MAR v3.14, HIRHAM5 and RACMO2.3 SMB values are extracted up to the grounding zone, thereby excluding the floating tongue, as determined by the catchment boundary of a previous study (*2*, *64*). Along catchment boundaries, the SMB value within each RCM cell is weighted proportionally according to the fractional area within the catchment polygon.

These catchment-integrated SMB values show that all RCMs have similar variability over time, despite their differences in temporal resolution. However, at times, the SMB estimates differ in magnitude by up to ~7 Gt yr^{-1} (Fig. 3B), and while HIRHAM 5 and MAR v3.14 data both show a declining SMB trend, RACMO2.3 data indicates no change over the investigated period. A previous comparison of the same three RCMs forced by a common large-scale Earth System Model found similar discrepancies in SMB between the RCMs on an ice-sheet wide scale (*65*). These differences in SMB were primarily attributed to differences in modeled runoff and meltwater refreezing within the firn. The discrepancies in modeled SMB magnitudes and trends that we present here emphasize that – while there have been transformative advances in RCMs in the past two decades – there remains considerable spread in their catchment-level assessments. More in-situ observations, including surface temperature and surface mass balance, and parameterizations, including meltwater runoff and refreezing, are still needed to improve RCM performance within the Petermann catchment (*66*).

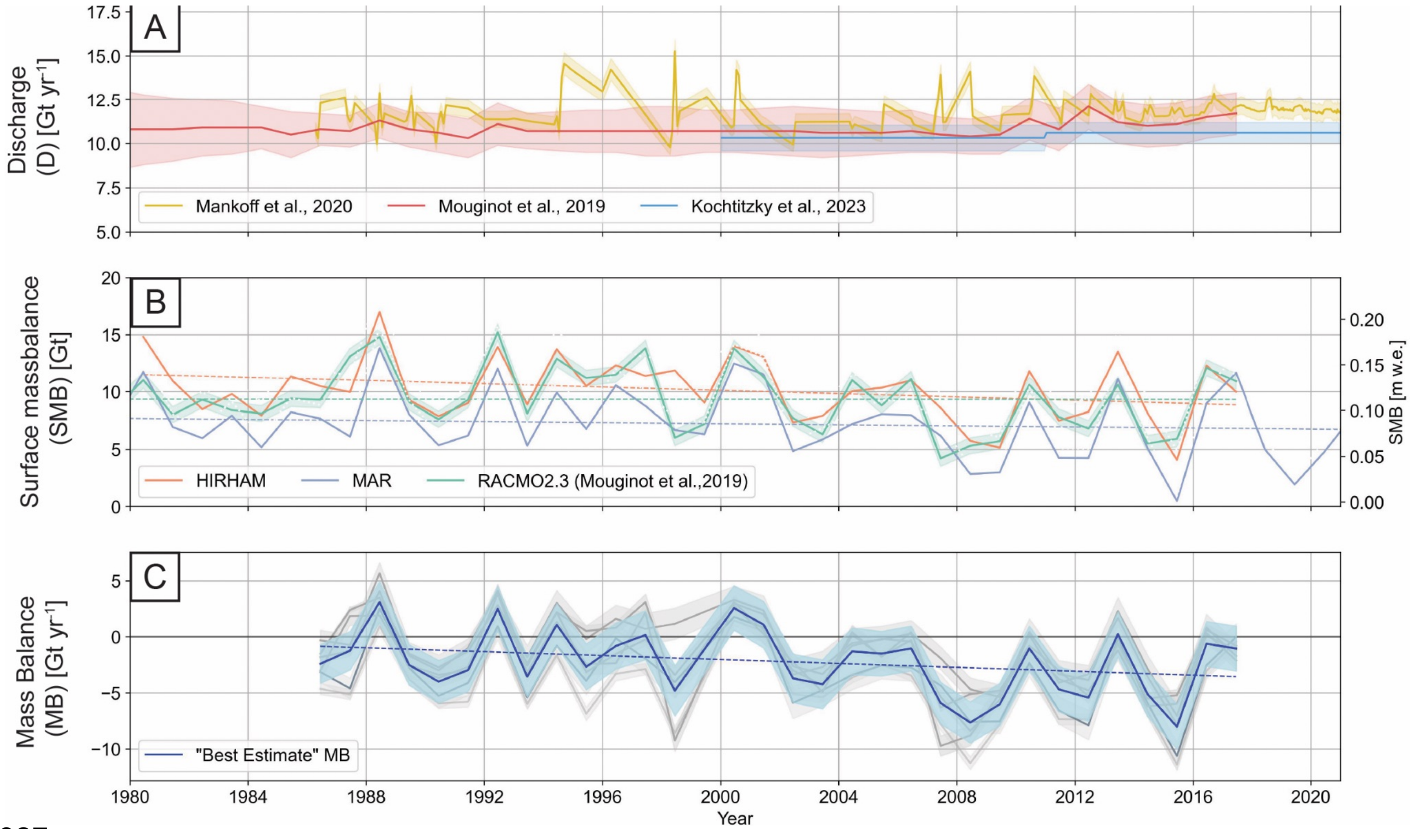

Figure 3 | Ice discharge, surface mass balance and mass balance for Petermann Glacier

*Comparison of **A)** monthly (yellow) (20, 21), annual (red) (2) and multi-decadal (blue) (22) ice discharge (D). **B)** Surface Mass Balance (SMB) from HIRHAM 5 (yellow) (61, 62), MAR v3.14 (blue) (63), and downscaled RACMO2.3 (green) (2, 55) with respective trendlines (HIRHAM 5 – dashed; MAR v3.14 – dash-dot; RACMO2.3 – dotted). **C)** Calculated mass balances shown in gray for combinations of D and SMB data products with "Best estimate" mass balance (MB) shown in blue and trend shown as dashed line.*

4. Ice–Ocean Boundary

Petermann Glacier's ice tongue extends into Petermann Fjord, which connects to Nares Strait (Fig. 4A). This ~500-km-long body of water separates Greenland from Ellesmere Island and connects the Lincoln Sea of the Arctic Ocean to Baffin Bay and the Atlantic

Ocean. Nares Strait is one of the major pathways for freshwater export from the Arctic Ocean, in the form of shallow, low-density polar water (*74*). However, northern and southern sills inhibit deep water throughflow in Nares Strait (Fig. 4B). The shallower southern sill prevents relatively warm Atlantic Water (AW, 2–3°C) traveling northward as part of the West Greenland Current from entering via Baffin Bay (*75*–*77*). Cooler AW (~1°C) that has transited the Arctic Ocean ascends the northern sill from the Lincoln Sea into Nares Strait (*20*, *75*, *78*). During this process, AW mixes with overlying water and cools by another 0.5 K (*20*). After entering Nares Strait, AW flows southward and spills over another sill to fill Petermann Fjord from about 400 m depth to the seabed (*48*). The sea ice state likely controls AW upwelling from the Lincoln Sea into Nares Strait and Petermann Fjord, with a mobile state leading to increased AW transport (*3*). Petermann Glacier's grounding line resides at a depth around 500 m (*43*), and undiluted AW has been observed up to 400 m depth within 3 km of the grounding line (*20*). This demonstrates the potential for a direct connection between melt rates along the base of Petermann Glacier's ice tongue and the temperature of AW in the Arctic Ocean. Long-term trends in AW conditions therefore exert a first-order control on the ice tongue stability and the larger glacier's mass balance.

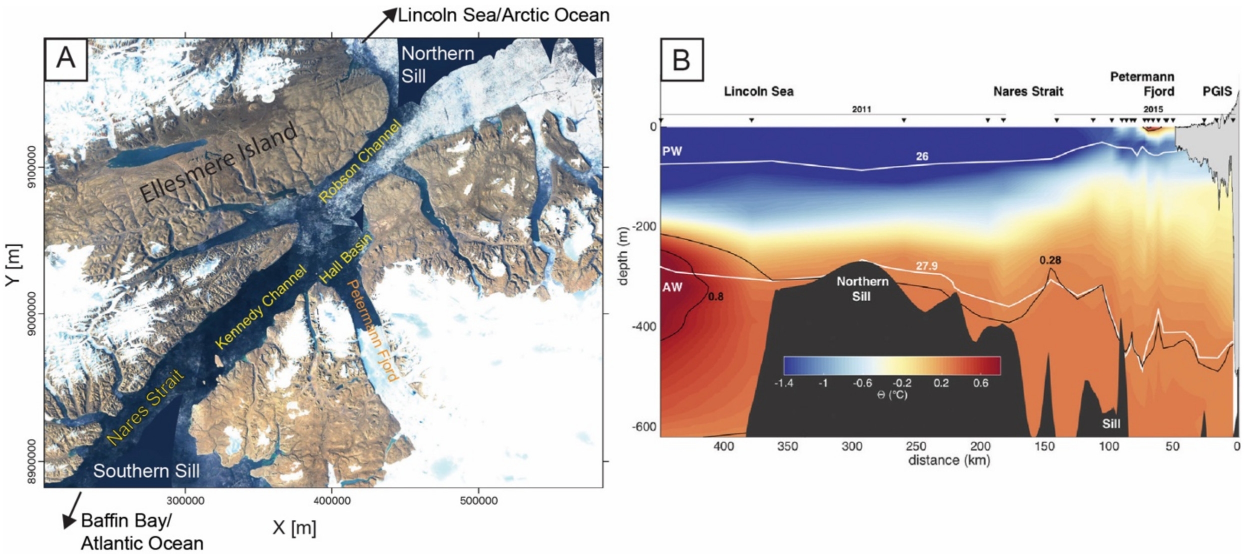

Figure 4 | Oceanographic overview

A) *Overview of Petermann Fjord in an oceanographic context. The X and Y axis are polar stereographic coordinates (EPSG:3413). Basemap is a Sentinel-2 cloudless mosaic by EOX IT Services GmbH (Contains modified Copernicus Sentinel data 2016 & 2107).* ***B)*** *Conservative temperature with selected isotherms in black, isopycnals in white, and bathymetry only shown above 650 m (taken from* (*20*)).

Despite its primary role in driving mass loss, the ocean cavity beneath floating ice shelves and ice tongues is significantly underconstrained due to the sheer difficulty in observing it. Access to the ice–ocean interface typically requires a substantial logistical undertaking, such as using hot water to drill through the ice, or deploying underwater robotic vehicles from a ship at the ice front (Jennings et al., 2022; Washam et al., 2019; Rignot et al., 2025). The observations that have been made beneath ice shelves and ice tongues expose a host of physical processes occurring across a range of scales that transport oceanic heat towards the ice to drive melting. Ocean-driven melting along the base of Petermann Glacier's ice tongue removes the majority of its mass (*36*) and the ice tongue has been thinning since 2007 due to increased basal melting (*30*). This mass loss highlights the importance of understanding key processes occurring at the ice–ocean interface for projecting the future behavior of this Greenland outlet glacier. In this section, we review the pathways of ocean heat delivery into and meltwater export from the Petermann Glacier's ice tongue cavity, dominant processes responsible for mixing ocean heat into contact with the ice base, and long-term trends in environmental forcing. We then summarize the lessons learned from these results and place them into context of the future stability of the ice tongue.

4.1 Oceanographic data

4.1.1 Pathways of ocean heat delivery and freshwater export in Petermann Fjord

The ice tongue of Petermann Glacier presently thins from ~600 to <100 m thickness over its ~50 km length , with much of this thinning occurring within 10 km of the grounding line in large channels melted into the ice base (*74*). Several studies spanning the time period of 2002 - 2022 have used remote sensing to map the melt rates across the extent of Petermann Glacier's ice tongue that lead to its distinct geometry (Ciracì et al., 2023; Münchow et al., 2014; Rignot & Steffen, 2008; Wang et al., 2024; Wilson et al., 2017). While the methods combined ice surface velocities with either direct ice thickness measurements from penetrating radar (Münchow et al., 2014; Rignot & Steffen, 2008) or digital elevation models that estimate the ice base from its surface (Ciraci et al., 2023; Wang et al., 2024; Wilson et al., 2017), the resultant melt rate distribution is qualitatively similar across studies. Maximum ocean-driven melting occurs in the inverted channels lining the ice base, with rates peaking around 100 m yr^{-1} (Fig. 5) (*4*). Strong melting concentrates within 10 km of the grounding line, where the majority of thinning occurs, then it diminishes considerably along the thin outer portion of the ice tongue. As the majority of Petermann's recent calving events have occurred in its outermost 20 km, they therefore only remove a relatively minor fraction of the ice tongue volume (*30*). However, intense channelized melting has been linked to rifting in Petermann Glacier's ice tongue via unstable distribution of internal strain induced by the large across-glacier thickness gradients (*75*, *76*) Melting along the ice tongue underside therefore directly affects its thickness and stability, which in turn dictate buttressing and the overall upstream glacier's current and future mass balance. This is of particular note, as average basal melt rates across the ice tongue appear to be increasing each year, resulting in unsteady thinning and potential destabilization (Wang et al., 2024). .

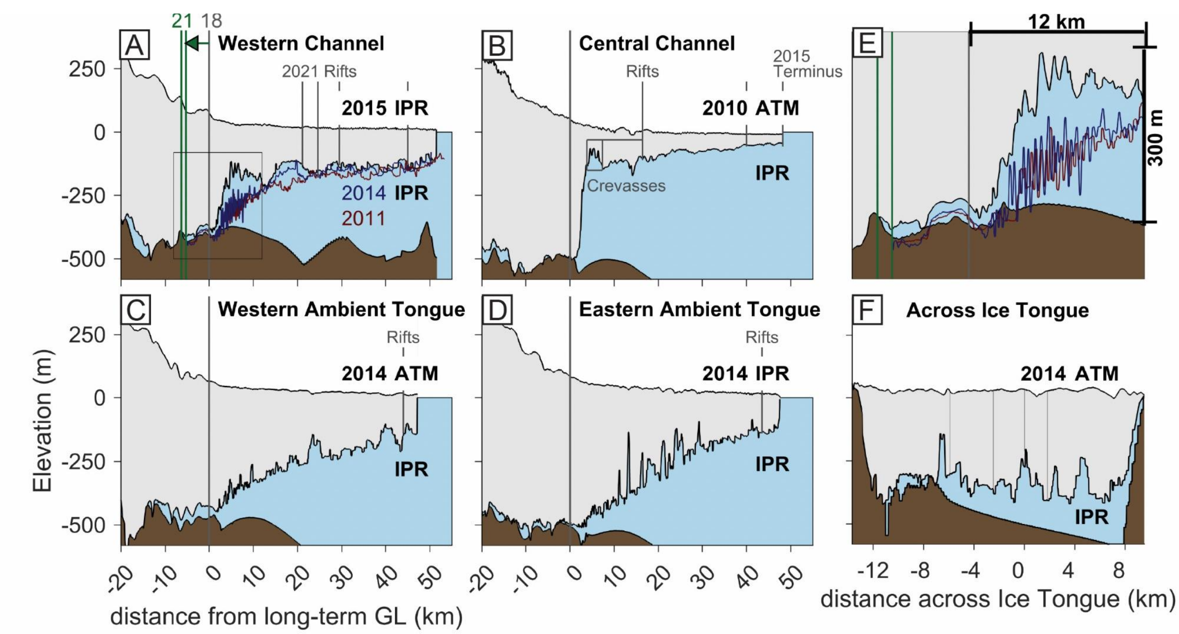

Figure 5 |Schematic of Petermann Glacier's floating tongue

Ice tongue geometry reveals concentrated melt near Petermann Glacier's GL. ***A -F)*** *Elevation profiles from the NASA/NSF OIB laser altimeter (ATM) and ice penetrating radar (IPR) from various years (flight lines in Figure 1) with the Bedmachine v3 bed, rifts, and 2015 terminus annotated.* ***E)*** *Focus on the 2018 – 2021 GL retreat and potential 2011 – 2015 thinning in the western channel. In* ***A), E)*** *the 2018 (grey line) and 2021 (green lines) GL locations are the intersections between the OIB flight lines and GL map in Figure 1.*

Local circulation within Petermann Fjord also controls ocean heat delivery to the ice tongue base and export of the resulting freshened meltwater–seawater mixture. As Petermann Fjord is ~15 km wide, or approximately twice the internal Rossby deformation radius, the Coriolis force influences fjord circulation and produces cross-fjord variability in water properties. In the northern hemisphere, the Coriolis force bends flow to the right, which concentrates deep AW inflow to the southwest side of the fjord and shallow meltwater-enriched outflow to the northeast (*40*, *41*). This cyclonic circulation results from cross-fjord density differences balancing pressure differences, referred to as the thermal wind balance. At marine-terminating glaciers, i ncreased freshwater release from melting and subglacial runoff leads to larger across-fjord density differences, which can increase ocean circulation strength, heat delivery, and meltwater export (*82*). All hydrographic sections in Petermann Fjord that resolve this density-driven circulation have been collected during the abbreviated summer season when air temperatures exceed freezing and freshwater release from melting and subglacial runoff are expected to be near their annual peaks. Importantly, this density-driven circulation is superimposed on background current patterns, of which there are no long-term measurements in Petermann Fjord. However, multiple observations suggest the importance of tidal interaction with density structure in Petermann Fjord, which drives ocean currents and internal waves (*41*, *83*). Such background circulation patterns likely dominate throughout much of the year when air temperatures remain below freezing. This summary highlights the large uncertainties that surround local fjord-scale processes, which control ocean transport below the ice tongue, where small-scale mixing ultimately determines the heat delivery to the ice–ocean interface and resultant melting.

4.1.2 Processes controlling melting beneath Petermann Glacier's ice tongue

Despite its remote location in northern Greenland, Petermann Glacier has been studied thoroughly with airborne radar sounding, in contrast to many other Greenland and Antarctic glaciers. This surveying has produced high-resolution ice thickness maps (Fig. 1C) that reveal four 200-m-tall and 1000-m-wide basal channels beneath its ice tongue (Fig. 5) (*36*, *74*), which are critical for its stability (*75*, *76*). Five boreholes have been drilled with hot water through the ice tongue to access the underlying ocean cavity. One of these was drilled in the northeastern shear margin of the outer ice tongue and four were drilled in the central basal channel between 3 and 26 km of the grounding zone. The resultant oceanographic and complementary phase-sensitive radar measurements have provided some of the most detailed observations of sub-ice oceanographic structure and ice-ocean interactions in basal channels.

. The water column cools and freshens above the thick layer of AW beneath Petermann Glacier's floating tongue , due to input of glacial meltwater and subglacial runoff, with all observations depicting a well-mixed upper ice–ocean boundary layer (*14*, *36*, *84*). Oceanographic instruments moored beneath the central basal channel showed that meltwater and subglacial runoff input creates a buoyant plume that occupies the boundary layer and flows seaward along the ice base (*14*). Current shear between the flowing plume and the immobile ice base mixes the upper boundary layer, driving ocean heat upwards towards the ice and diluting fresh meltwater into seawater. However, within 1 m of the ice base, the ocean restratifies, with significant cooling and freshening insulating the ice base and reducing melt rates (*83*). Nevertheless, the strength of the under-ice buoyant plume controls melting in the ice tongue central channel. Seasonal variability in subglacial runoff discharge from atmospheric melting plays the dominant role in driving the under-ice plume, with melt rates increasing by an order of magnitude in summer (*14*). Hydrological modeling suggests that the subglacial conduits that deliver fresh runoff to the grounding line are aligned with ice tongue channels (*35*), with the buoyant plume seeding their downstream evolution. These patterns link the channel melt rates to atmospheric forcing through the seasonal cycle in surface melting, subglacial runoff discharge flux across the grounding zone, and the strength of the meltwater plume (*85*).

Away from the vigorous outflowing plume, the steeply sloping sidewalls of the channels melt more rapidly than flat portions of the ice base (*86*), due to an interplay with ocean stratification that drives variable heat flux towards the ice (*87*). This feedback allows the channels to melt both outwards and upwards to erode the ice shelf laterally. Tidal currents in the grounding zone are also thought to drive vigorous melting through AW delivery (*4*, *15*, *16*) and modulate outflow of meltwater plumes (*83*). Hence, the dynamic ice–ocean interactions occurring in the grounding zone set the foundation for ocean circulation and melting beneath the Petermann Glacier ice tongue (*85*). Changes to the AW temperature and subglacial runoff flux generated during summer are therefore of primary importance for the ice tongue stability.

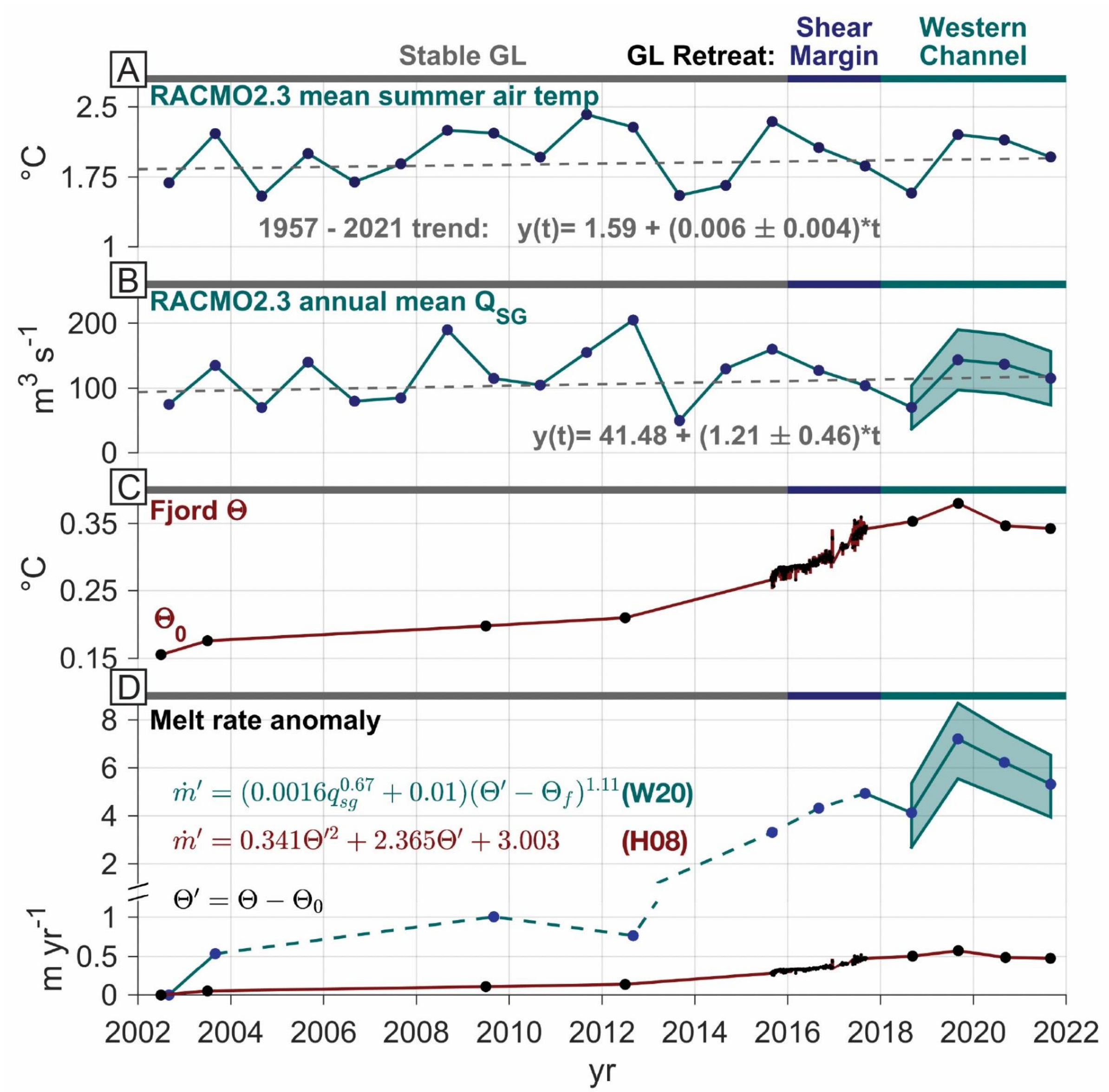

***Figure 6** | Ocean and atmospheric forcing on Petermann Glacier*

*Ocean and atmospheric forcing on Petermann Glacier for the period 2002 – 2021 using RACMO2.3 (55) data. **A)** mean summer 2 m air temperature output for Petermann near the GL and **B)** mean annual runoff for the upstream catchment that is assumed to discharge subglacially (Q_{SG}). **C)** Conservative Temperature (Θ) of Atlantic Water in Petermann Fjord. **D)** Bulk ice shelf melt rate anomalies considering ocean warming (Figure 5a of (88)) and ocean warming combined with SGW flux through the western channel (Eqn. (10) of (83), adapted for Θ'). Q_{SG} values have been multiplied by 0.555, following (4), and a channel outlet cross-section area of 707 m^2, following (83), to account for the two main SGW outlets at the GL.*

4.1.3 Impacts of long-term trends in ocean and atmospheric on melt rates

A collection of in situ oceanographic observations and atmospheric reanalyses tracks the long-term environmental forcing impacting Petermann Glacier, including during the 2016–

2021 period when its grounding line retreated (Fig. 1) (*9*). Mean summer air temperatures near the grounding line, estimated by RACMO2.3, increased significantly between 1957 and 2021 (Fig. 6 A). The summertime atmospheric warming affected a large area of Petermann's catchment and likely increased the annual average subglacial runoff flux across the grounding line (Q_{SG}) by 77 ± 29 m^3 s^{-1} over these 64 years (Fig. 6 B) (49). Remote sensing likewise indicates expanded surface melt area in northern Greenland (*48*). In addition to a warming summer season, AW temperatures increased by 0.2 K in Petermann Fjord, from 0.15°C to 0.35°C between 2003 and 2021 (Fig. 6 C).

After remaining stable for the satellite observational period, Petermann Glacier's grounding line began retreating along its shear margins in 2016 (*9*), coincident with a marked upturn in AW temperature (Fig. 6 C). The grounding line then started retreating along the western ice tongue channel in 2018 (Fig. 5) (*9*) when AW temperatures reached 0.35°C. This grounding line retreat coincided with a 15% increase in ice flow speed (*9*), which suggests that the retreat initiated an inland response. Area-averaged ice tongue melt rate relations, based on the observed ocean warming (*88*) and the combination of ocean warming and greater subglacial runoff (SGW) discharge from warmer summers (*83*), reveal the importance of SGW-induced circulation to melting (Fig. 6 D). Notably, the long-term melt rate anomaly in regions of Petermann Glacier's ice tongue influenced by SGW discharge is an order of magnitude higher, at 6–8 m yr^{-1}, than the ~0.60 m yr^{-1} across the rest of the ice tongue that is exposed only to ocean warming.

Repeat-pass radar surveys of Petermann Glacier's western ice tongue channel suggest that it thinned by up to ~150 m between 2011 and 2015, within 12 km of the now-retreating grounding line (Fig. 5 E). Track alignment errors between flights are small (21 ± 4 m, 95% confidence interval), but steep thickness gradients along the channel sidewalls (Fig. 5 F) could have caused even these small misalignments to manifest as a false thinning signal. Evidence from multiple independent datasets indicate that increased SGW discharge in the western channel has accelerated localized melting and driven GL retreat. The bed slopes downward up-glacier of the last observed GL location (2021), suggesting that further retreat may be ongoing (Schoof, 2007). Combined ocean warming and increased SGW discharge are likely increasing melt rates and thinning the other ice tongue basal channels in a similar fashion. This unstable channelized thinning increases internal strain in Petermann Glacier's ice tongue (*75*) and is contributing to the multiple rifts present in the ice tongue (*76*, *84*). The proliferation of rifts has the potential to accelerate calving and destabilize the ice tongue. Recent modeling shows that if the ice tongue totally collapses, the grounding line will retreat and Petermann Glacier's ice flux will increase by 40%, substantially raising sea level (*89*). This highlights Petermann Glacier's vulnerability to ongoing ocean and atmospheric warming that combine to drive melting along the ice–ocean boundary.

4.3 Terminus processes

We use terminus positions from the TermPicks dataset (Fig. 1A) (*17*, *18*) and the centerline method within the Margin Change Quantification Tool (MaQiT) (*19*) to assess Petermann Glacier's terminus position change between 1970 and 2015. Few observations of terminus positions exist prior to the satellite era (*29*) so it is difficult to definitively determine terminus change before 1970. However, previous studies suggest that large calving events at Petermann Glacier occurred with a 5–10 year frequency with periods of steady advance with a rate of ~1 km yr^{-1} since the first observations in 1876 (*8*, *29*, *90*). The dominant calving style at Petermann Glacier is tabular rifting, similar to other glaciers with a floating ice tongue in Greenland as well as Antarctica ice shelves, where a rift propagates across an ice shelf until it reaches full width (Humbert et al., 2023; *Bezu and Bartholomaus, 2024*). Between 2000 and 2010, the terminus of Petermann Glacier has been relatively stable, except for interruptions by comparatively small calving events. In the following decade, significant calving events in 2008, 2010 and 2012 resulted in large-scale terminus retreat (Fig. S1A). The latter two events have been associated with the early break up of landfast sea ice, which usually provides backstress on the glacier terminus and inhibits calving (Detlef et al., 2021). Landfast sea ice has also been shown to prevent the inflow of warmer Atlantic Water into Petermann Fjord (Shroyer et al., 2017) and mélange from exiting Petermann Fjord thereby not only impeding calving, but also basal melting of the floating tongue (Akesson et al.,2022). A similar scenario has been observed at Ryder Glacier, North Greenland, where tabular icebergs are trapped within the fjord by sea ice, thereby providing backstress and reducing calving (Jakobsson et al., 2020).

While large calving events have been observed in the past, these three events suggested an increase in periodicity attributed to weakening of the floating tongue through basal melting (*33*, *90*). However, the large calving event that is currently underway, which followed a steady advance of ~10 km since 2012 (Fig. S1, S5), is more consistent with the calving frequency and dynamics found prior to 2010. If future large calving events were to follow this current event, analogous to the 2010–2012 period, they could reach the critical distance to the grounding zone of ~12 km in 5–10 years and lead to additional inland acceleration and increased ice discharge of (*6*).

The period of glacier advance between 2012 and 2025 contrasts with the previously discussed SMB decline (section 3.32), but appears to coincide with an increase in subglacial runoff, which is extracted as a weighted catchment average from 1 km monthly MAR v3.14 data (*63*) and converted from millimeters water equivalent per month to gigatons per year using the catchment area determined by a previous study (*2*, *55*). Subglacial runoff appears to be relatively low from 1970 until approximately mid-2000, when it starts to slightly increase (Fig. S1C). Comparatively higher summer runoff peaks are apparent in 2014 (4.6 Gt yr^{-1}) and 2020 (5.2 Gt yr^{-1}), and a slight increase in annual mean runoff is apparent over the investigated period. A recent modeling study found the presence of a distributed water sheet, which persists year-round within 20 km of the grounding zone, but extends far inland during the melt season with a thickness of several centimeters (*35*). The same study also suggests that the highest subglacial runoff rates are found within the five channels that are distributed across the grounding zone, where peak runoff rates can exceed 100 $m^3\ s^{-1}$ during the melt season (*35*).

While terminus positions can be readily derived from remote sensing data, additional observations of subglacial runoff, especially within and upstream of the grounding zone, are needed. These would help to not only better constrain basal and submarine melt rates, but also to provide further insights into the advance and retreat behaviour of Petermann Glacier.

5. Ice–Bed Boundary

Processes that occur at the ice–bed boundary are still poorly understood, as the collection of direct observational data there remains challenging. In this section, we discuss recent advances in geophysical data interpretation, which provide a more holistic perspective of the state of Petermann Glacier's ice–bed interface, with the aim to provide novel insights and to discuss the potential implications for its stability.

5.1 Geology and Geothermal History

The first map of Greenland's subglacial geology highlighted that the geology beneath Petermann Glacier and its catchment region was both likely complex and poorly constrained (*94*). A more recent synthesis, based on available geophysical data, suggests the Petermann Glacier catchment is underlain by at least three distinct geologic provinces (Fig. 7 A) (*95*). The subaerial geology bounding Petermann Glacier's land-terminating margin and floating ice tongue is the Franklinian Basin, which comprises sedimentary shelf and basin deposits (primarily limestone) of 560–410 Ma age and outcrop spectacularly along the flanks of Petermann Fjord. The Franklinian Basin likely underlies the lower fifth of its ice-sheet drainage basin. Farther inland, underlying approximately the next two-fifths of the basin, is the Inglefield Orogen, which is a predominantly Archean basement with subsequent Paleoproterozoic orogenic activity. The subglacial geology in the uppermost fifth of the ice-sheet catchment is unclear, as its large-scale geophysical properties are not yet clearly reconcilable with more peripheral regions that have subaerial exposures. Neither the boundary between the Inglefield Orogen and this unknown central region nor the boundary between the Franklinian Basin and the Inglefield Orogen are particularly well defined.

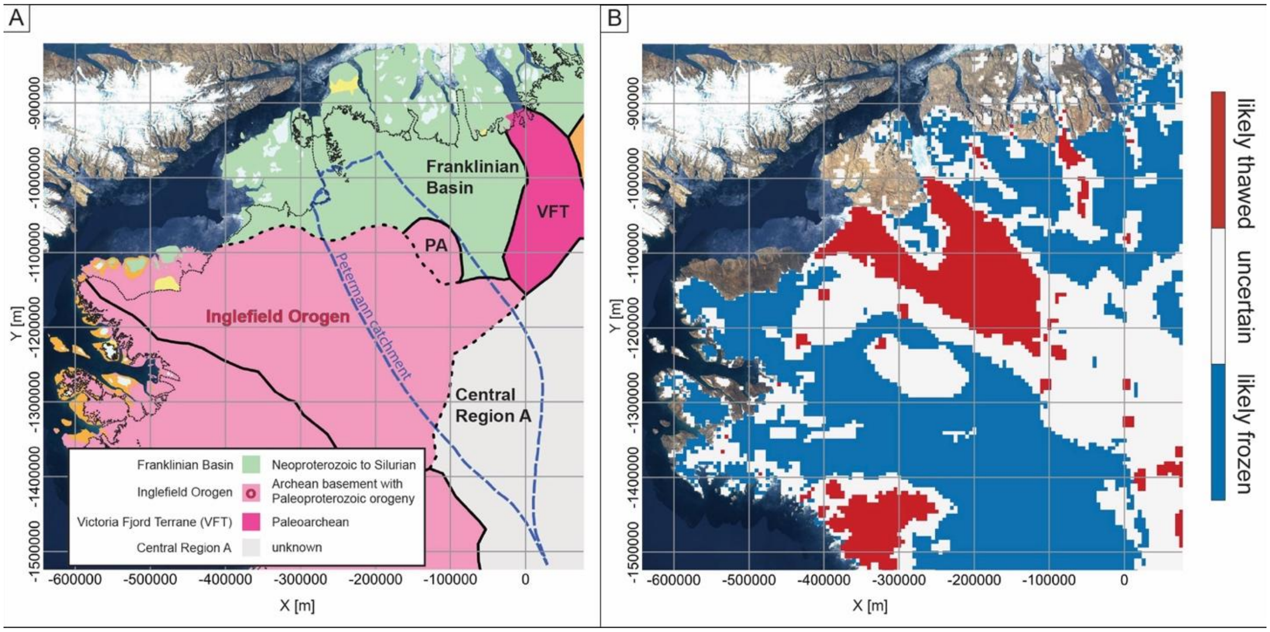

Figure 7 | Geology and basal thermal state

A) *Geological provinces in Greenland after (95) with Petermann catchment outlined as dashed blue line (64) and 2015 ice extent shown as dotted line (96). PA refers to the Petermann anomaly.* ***B)*** *Basal thermal state of the Greenland Ice Sheet after (97). Basemap is a cloudless Sentinel-2 mosaic provided by EOX IT Services GmbH. The X and Y axis are polar stereographic coordinates (EPSG:3413)*

The widespread presence of subaerial basalt and porphyry erratics around the ice margin in Northwest Greenland, with no corresponding subaerial source, led a previous study to hypothesize the presence of a subglacial volcanic source province in the region (*94*). With geophysical data synthesis, it is apparent that there is an unusual ~4,000 km^2 elevated bedrock feature within the Inglefield Orogen, referred to as the "Petermann Anomaly" (PA; Fig. 7 A) (*95*). Its relatively high gravity and magnetic anomalies suggest a batholith, possibly formed during the transit of the Iceland Hotspot (*98*). A previous study inferred that the Iceland Hotspot transited near Petermann's grounding zone at ~75 Ma, likely causing partial melting of the lithosphere, or intrusion into the lower crust (*99*). They also inferred an enhancement of present-day geothermal heat flow at Petermann Glacier's grounding zone (~ +10 mW m^{-2}). However, other models infer no discernible heat flow enhancement there, suggesting instead that inferences of enhanced heat flow from lithospheric modelling may reflect paleoimprints on underlying lithospheric architecture (*100*). While it is plausible that the Petermann Anomaly is a batholith associated with the Iceland Hotspot transit, a batholith is a poor match for the porphyry erratics described by (*94*). This ambiguity suggests that there may be an additional, as-of-yet unidentified subglacial volcanic province, in the vicinity of Petermann Glacier (*101*).

5.2 Ice Stream Onset

Compared to most other Greenlandic outlet glaciers, Petermann Glacier has an unusually localized onset of fast ice flow that can be traced to a ~10 × 10 km region directly adjacent to the Petermann Anomaly, roughly ~220 km upstream of the grounding zone (Fig. 8 A). This highly localized onset of fast flow is similar to that of the Northeast Greenland Ice Stream and Antarctic ice streams (NEGIS; Fig. 8 B, S5), whereas for virtually all other Greenlandic outlet glaciers, surface speeds increase gradually over tens to hundreds of kilometers. Ice streams are typified by high inland surface ice velocities yet low driving stresses, with well-defined shear zones (*102*). This mechanism of achieving fast inland flow contrasts substantially with that of Sermeq Kujalleq (Jakobshavn Isbræ), where instead ice flow is channelized within deeply incised subglacial channels and where higher inland ice velocity is driven by higher driving stresses, and where ice–ice shear zones are typically less well-defined (Fig. 8 C) (*102*). In contrast to Sermeq Kujalleq, the onset of fast flow at both Petermann Glacier and NEGIS appears to be mostly independent of local spatial variability in subglacial topographic roughness or a deep subglacial channel (*95*, *103*), although the northeastern flank of Petermann Glacier's onset region is bounded by the Petermann Anomaly. Given the clear analogue of Petermann's fast flow onset, its pronounced shear margins, and elevated basal slip ratio similar to both NEGIS and other Antarctic ice streams, we hereafter refer to "Petermann Ice Stream", to more accurately reflect its apparent dynamics (*104*).

There are several significant implications to reclassifying Petermann as an ice stream. Due to their high velocities at low driving stresses, ice streams are generally considered to be less stable than topographically constrained outlet glaciers, meaning that they can both accelerate or decelerate relatively rapidly (*105*, *106*). Recent radiostratigraphic analysis suggests that two ice streams used to flow into Nioghalvfjerdsbræ (79N Glacier) earlier during the Holocene, before shutting down before ~2.5 ka (*107*). The relatively recent shutdown of these northeastern ice streams appears to have caused the main drainage system to reconfigure and possibly lead to the enhancement of ice flow at NEGIS. This reconfiguration highlights the potential sensitivity of Greenland ice streams to reorganize over relatively short timescales, and that the ice flow observed at Petermann today may not reflect past discharge across the grounding zone, which presents a challenge for the use of recent observations to calibrate projections of ice sheet form and flow (*108*).

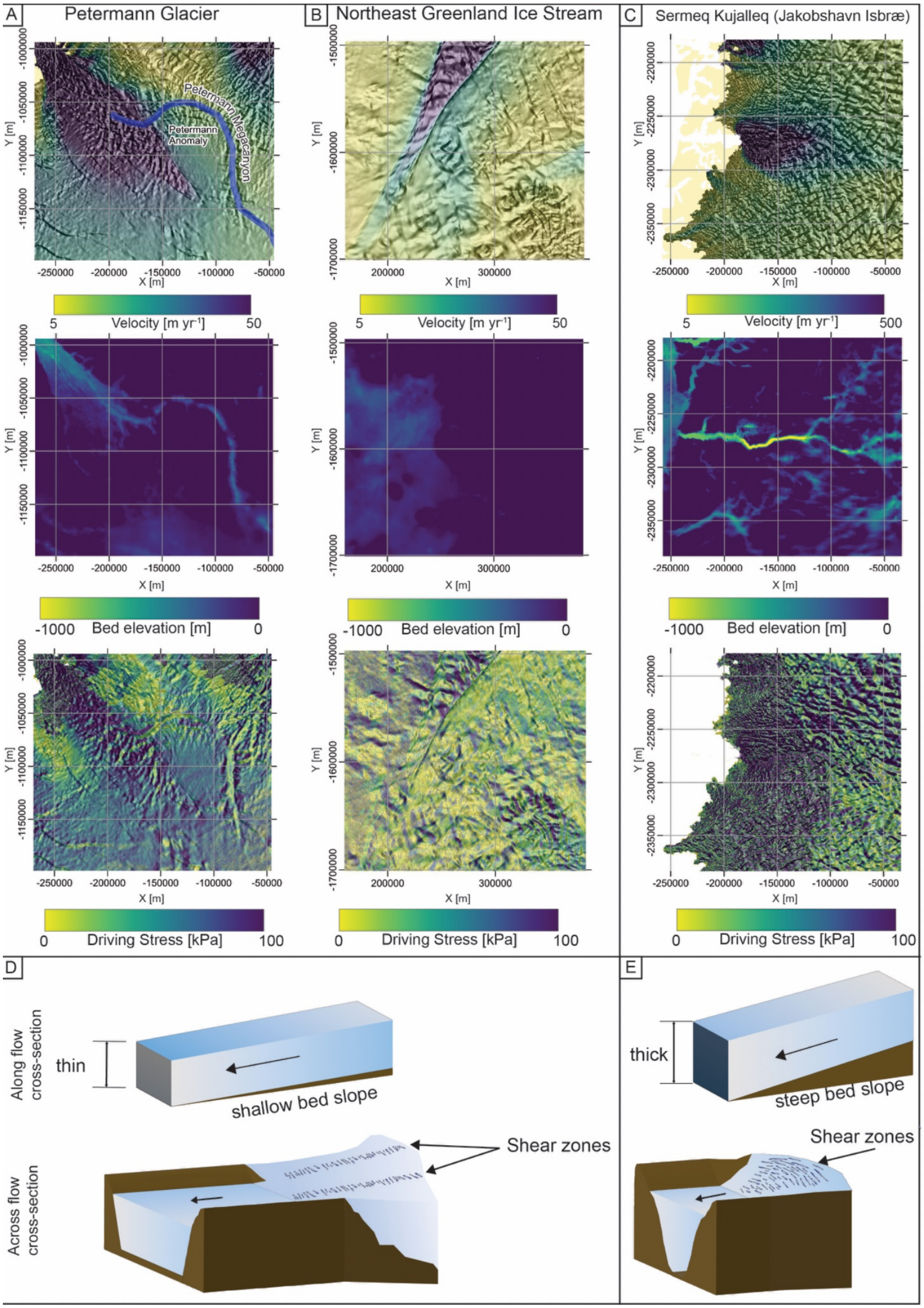

667 ***Figure 8 | Ice stream vs isbræ***

Flow-aware hillshade that mostly highlights the surface expression of basal topographic relief (*95*) *overlaid with a MEaSUREs multi-year velocity mosaic* (*109*, *110*) *bedrock topography from BedMachine v5* (*24*, *25*) *and driving stress calculated from BedMachine v5 and MEaSUREs multi-year velocity mosaic for* ***A)*** *Petermann Glacier with megacanyon indicated in blue,* ***B)*** *Northeast Greenland Ice Stream (NEGIS), and* ***C)*** *Sermeq Kujalleq (Jakobshavn Isbræ; Note the different color scale for velocities). Conceptual sketch for along flow and across flow cross sections for* ***D)*** *Ice Streams and* ***E)*** *isbræs. The X and Y axes are polar stereographic coordinates (EPSG:3413).*

5.3 Ice velocity

We review the agreement between the MEaSUREs v5 (*23*, *67*, *68*) and PROMICE v4 (*69*, *70*) ice velocity data at Petermann Glacier. The MEaSUREs v5 velocity product is derived from TerraSAR/TandDEM-X as well as Landsat-8 and -9 optical imagery and is available at a monthly resolution. PROMICE v4 data is derived solely from Sentinel-1 synthetic aperture radar imagery and has a temporal resolution of ~11 days. Velocities for both datasets are extracted along a Petermann Glacier centerline that has been delineated from the ice flow direction using PROMICE v4. Landsat-derived ITS_LIVE (*71*, *72*) is an additional velocity product that could be used, however data is only available on an annual resolution , so we chose not include it in this comparison.

Both the MEaSUREs v5 and PROMICE v4 ice velocity products capture the general spatial pattern in ice velocity along the centerline during the 2016–2024 period. The annual mean velocities for both data products (Fig. 9) show that velocity variability is highest at the terminus and decreases towards the interior of the GrIS. The mean ice flow velocities only disagree by 24 m yr^{-1} (~2%) over this centerline profile (MEaSUREs v5: 1131 m yr^{-1}; PROMICE v4: 1155 m yr^{-1}; Fig. 9 A-C, B).

While both satellite-derived ice velocity products appear to agree well when averaged over 2016–2024, their annual mean and maximum velocities exhibit a significant divergence after 2021 (Fig. 9 D, C). The divergence in mean velocity grows to ~34 m

yr^{-1} by 2024. While maximum MEaSUREs and PROMICE velocities generally agree before 2021, after 2021 maximum PROMICE velocities increase steadily from ~1331 m yr^{-1} to ~1490 m yr^{-1} (11.9%). In contrast, maximum MEaSUREs velocities increase only marginally between 2021 and 2023 from ~1316 m yr^{-1} to 1329 m yr^{-1} (0.99%) and then decrease to ~1290 m yr^{-1} (2.9%) in 2024. This results in an appreciable difference in maximum flow velocity of 199135 m yr^{-1} (~13.4 %) between data products.

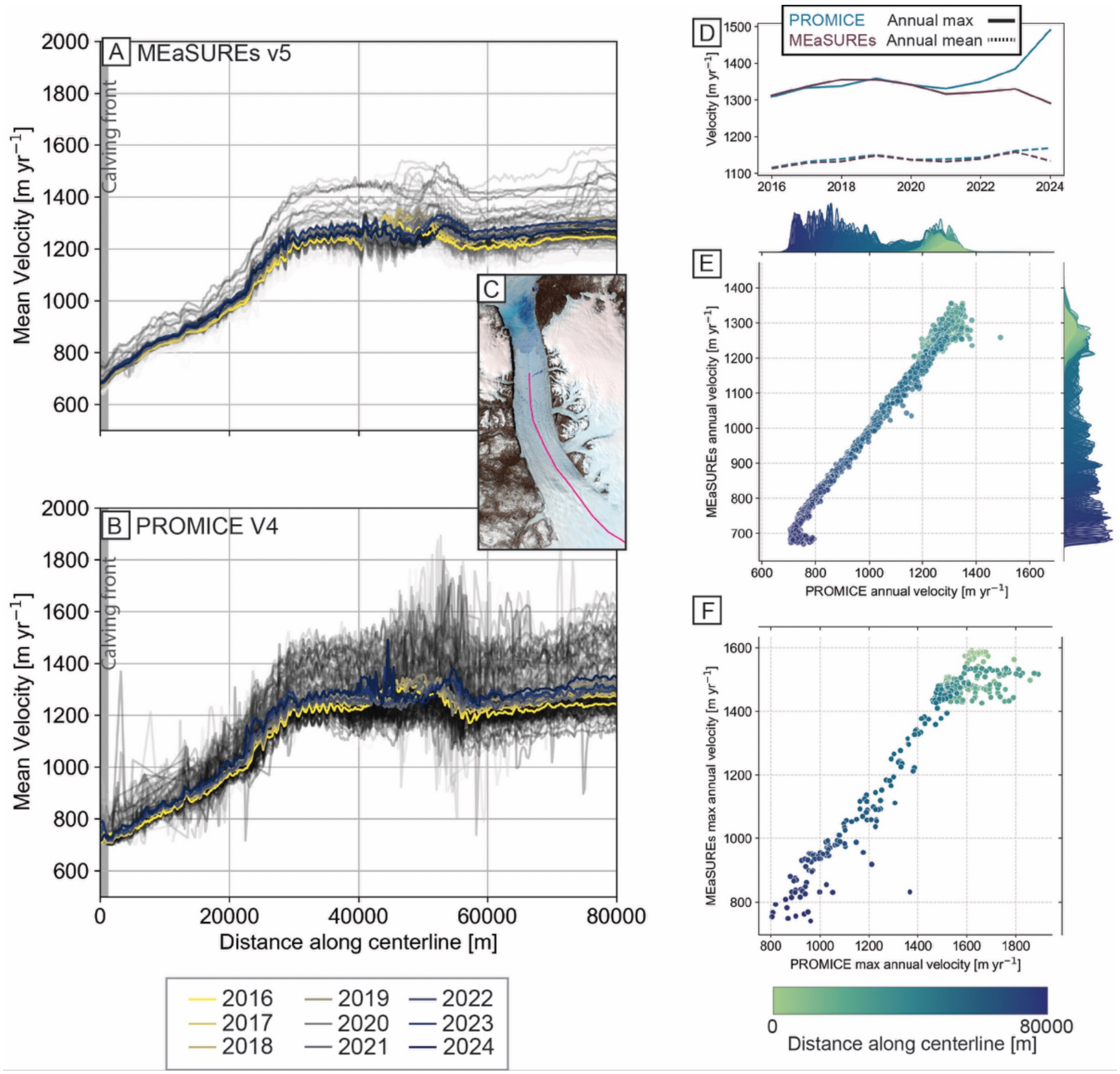

Figure 9 | Petermann Glacier flow velocities

*Comparison of MEaSUREs v5 (23, 67, 68) and PROMICE V4 (69, 70) centerline velocities. **A-B)** All available velocities extracted along the centerline shown in grey for MEaSUREs and PROMICE, respectively. Annual velocity averages shown with color indicating the year (yellow= 2016, blue=2024). **C)** Inset map shows location of the centerline along which velocities are extracted. Basemap is a pan-sharpened Landsat-8 image from 17/06/2024. **D)** Annual mean (dashed line) and maximum (solid line) ice velocities from MEaSUREs v5 (purple) and PROMICE V4 (teal) extracted along the centerline between 2016 and 2024. **E)** Linear regression of MEaSUREs and PROMICE mean ice velocities grouped by year and distance along the centerline. Marker color shows distance along the centerline, and histogram shows distribution of data points with color indicating distance along the centerline. **F)** Linear regression of MEaSUREs and PROMICE maximum ice velocities grouped by distance along the centerline. Marker color shows distance along the centerline.*

The linear regression between MEaSUREs v5 and PROMICE V4 grouped by year and distance along the centerline (Fig. 9 E, D) indicates a comparatively large spread within the first 30 km from the terminus. Compared to MEaSUREs v5, the PROMICE v4 velocities appear biased towards higher velocities downstream of the grounding zone. Similarly, maximum velocities have the largest variability at the terminus (Fig. 9 F, E) and past the grounding zone, with PROMICE v4 velocities being again higher than MEaSUREs v5.

This comparison of velocity products shows that data with sub-monthly temporal resolution is able to capture the spatial variability of velocities across the floating tongue, which is not resolved in the monthly data (Fig 9 A, B). The variability is likely also reflected in the annual mean and maximum velocities (Fig 9. D, F), thus suggesting that high-temporal resolution data might be more suitable to investigate changes in flow. It further highlights that ice velocities at Petermann Glacier have a strong seasonal variability, which is consistent with previous studies which found a 10–15% increase in velocity during the summer since 2013 due to reduced basal friction moderated by changes in subglacial hydrology (*9*, *35*). Between 2015 and 2018, winter velocities increased by approximately 10%, which was attributed to the loss of ice shelf resistance following the 2012 calving event (9). The winter speed-up is also consistent with the suggestion that Petermann Glacier follows a pattern of short-lived glacier acceleration followed by sustained high velocities for several years after a retreat, which has also been observed at other glaciers with floating tongues in Greenland (*73, Hill et al., 2018*). The loss of ice shelf buttressing has also been associated with additional thinning and grounding line retreat in 2017/2018 (*9*). The 2015 speed-up also coincided with the development of two distinct, flow-parallel shear zones on the ice tongue, which caused a velocity gradient across the ice tongue (*9*). After 2018, velocities have remained relatively stable, despite rapid grounding line retreat on a retrograde slope (*9*). While the velocity data products shown in Fig. 9 are generally in good agreement with each other, the difference in maximum velocity as well as the spread of maximum ice velocities at the terminus indicates that – when seasonal variability is not accounted for – ice velocities are underestimated. Ice velocity products that resolve seasonal variations are therefore preferred for investigating ice dynamics at Petermann Glacier.

5.4 Basal Topography

The bed topography at Petermann Ice Stream makes it prone to large dynamic mass loss, as its shallow slope has the potential to cause drawdown from dynamic thinning farther inland (*111*, *112*). A previous study (*112*) identified knickpoints, which are rises in the bed topography that act as natural limits for inland thinning, and found that the thinning limit for Petermann Glacier, similar to Humboldt Glacier, would be more than 200 km from its current grounding line. Thus, should Petermann Ice Stream experience increased basal melting and dynamic thinning, this could result in s lower, but more sustained long-term mass loss through inland thinning (47, 111,112). The interior of the GrIs has also been identified as the area that holds the majority of committed future sea level rise, with Petermann Ice Stream contributing up to 0.65 mm by 2100 under high basal melt scenarios (47, *113*, *114*). Conversely, Sermeq Kujalleq (Jakobshavn Isbræ) and NEGIS have distinct knickpoints that limit dynamic thinning to within <150 km of their margins, but their respective high ice flux of more than 15 Gt yr^{-1} also indicate the potential for large future dynamic mass losses (*112; Rignot et al., 2000; Schlegel et al., 2014; Hansen et al., 2021*).

The most pronounced subglacial topographic feature beneath Petermann Ice Stream is the ~1700-km-long megacanyon, which is incised about ~0.5 km into the local bed topography (*24*, *25*, *44*). During interglacial periods, assuming an ice-free Greenland with rebounded bedrock topography, this canyon would have drained ~25% of Greenland's area, reaching as far south as ~68°N (*115*). While one study (*44*) argues that it was likely carved via fluvial activity through many glacial cycles, another study (*116*) highlights the possibility that the canyon may be much younger, incised during Pliocene–Pleistocene megafloods, although this interpretation is disputed (*116*, *117*). For either interpretation, the megacanyon is agreed to be fluvial in origin and to predate the formation of the Greenland Ice Sheet. The megacanyon is clearly deflected around the Petermann Anomaly, which suggests that the latter's rock is more competent than its surroundings (*95*). This pattern also indicates that the Petermann Anomaly predates the formation of the megacanyon.

5.5 Subglacial Hydrology

The megacanyon likely collects subglacial meltwater from a large portion of the present-day ice sheet, ultimately influencing subglacial hydrology over (*35*, *44*). Presumably, channelized subglacial runoff of this meltwater at the grounding zone induces additional basal melting of deep longitudinal channels into the bottom of the downstream ice shelf (*36*). The ISMIP6 ensemble of ice sheet models suggests that Petermann's ice-sheet catchment is thaw-bedded inland (Fig 7B) to near the ice stream onset (~2000 m surface elevation) (*97*). Farther inland, the synthesis basal thermal state does not agree with the ISMIP6 ensemble, and it is unlikely that the bed is thawed along the megacanyon's entire length. Although the grounding zone of Petermann Ice Stream is partly formed and constrained by the megacanyon, it only intersects with the megacanyon ~100 km downstream of the onset of its fast flow (*103*). The relatively deep megacanyon underlying the lower reaches of Petermann Ice Stream contributes to strong seasonal variations in velocity associated with surface-driven seasonal variations in subglacial hydrology (*35*). Efficient subglacial drainage may also contribute to the absence of observed subglacial lakes within the Petermann Ice Stream catchment, despite relatively extensive airborne radar sounding there that should be able to otherwise identify these features (*118*, *119*).

The catchment of Petermann Ice Stream contains perhaps the densest concentration in Greenland of disrupted basal ice units observed by radar sounding (*104*, *120*). While these deeper radiostratigraphic anomalies may be due to large-scale folding induced by anisotropic ice flow (*121*), they may also be due to either surface or basal meltwater refreezing at the ice–bed interface (*122*, *123*), or perhaps even localized convection (Law et al., 2026). If these basal stratigraphic anomalies are indeed associated with refreezing meltwater, it would suggest that basal water is more widespread than inferred by the ISMIP6 ensemble. It would also suggest the possibility of more extensive enhanced warming and deformation of basal ice. At the same time, however, pre-Holocene ice outcrops are extensive along the land-terminating ice margin between Petermann Ice Stream and Humboldt Glacier (*124*). These ice outcrops imply that at least some pre-Holocene ice experiences little basal melt and reaches the ice margin in close proximity to the ice stream's thawed bed. Together, these inferences suggest large spatial gradients must exist in Petermann Ice Stream's basal thermal state (*120*).

Subglacial runoff is expected to increase in the future, with increasing air temperatures and Arctic Amplification, which could lead to an earlier onset of the melt season (*48*, *49*, *91–93*). As a result, the distributed subglacial water sheet, discussed in section 4.3, might extend even farther inland, thereby increasing basal motion in previously low friction areas and sustaining higher velocities. Higher subglacial runoff could also have implications for the subglacial hydrological system, which could develop a more efficient, channelized drainage system that can drain higher influxes of subglacial runoff (*35*). While this might suggest an earlier onset of the seasonal speed-up and higher velocities throughout the melt season, further measurements are needed to confirm this hypothesis (*35*). A future increase in runoff could also lead to enhanced basal melting of the floating tongue through a stronger buoyant plume as discussed in section 4.1 (*42*, *85*).

6. Projected Mass Loss and Sea Level Rise

The drainage basin of Petermann Glacier holds approximately 0.38 m of global mean sea-level rise, which has motivated extensive modeling efforts exploring how different mass-loss mechanisms may influence the glacier's stability. One modeling study found that an immediate collapse of the ice tongue would contribute 0.92 mm to global sea level rise, by increasing flow velocities and ice discharge, forcing grounding line retreat and thinning (Hill et al., 2021). Calving has been shown to have a minor effect on grounding line retreat, except when it occurs within proximity of the grounding zone (Nick et al., 2012, Hill et al., 2018, 2021). A modeling study showed that should calving occur within 12 km of the grounding zone the loss buttressing would result in an increase of flow speeds by an average of 0.9 km yr^{-1} and an increase in ice discharge from 11 Gt yr^{-1} to 25 Gt yr^{-1} , which is equivalent to 0.07 mm yr^{-1} of sea level rise (Hill et al., 2018). Similarly, increases in surface melt and doubling of the melt season appear to have little effect on grounding zone position, even though reduced basal friction leads to an initial doubling of ice discharge, which gradually decreases as the glacier adjusts to its new geometry (Nick et al., 2012).

On the other hand, submarine melting has been found to have a significant impact on the future stability of Petermann Glacier and its floating tongue (Nick et al., 2012, Akesson et al., 2021). A tripling of submarine melt rates, comparable to that observed between the 1990s and early 2020s, was found to result in an ice discharge increase by ~300% in less than a millenium with extensive retreat of the ice shelf (~40 km) and grounding zone (~80km) (Nick et al., 2012). Another study found that an immediate increase in ocean forcing alone can force the break-up of the ice shelf and would lead to a maximum contribution of 11 mm of global sea level rise by 2300 (Akesson et al., 2021). They also found that the contribution to sea level rise from increased ocean forcing depends on the basal friction, with a warming of 2 K leading to a 2.3–6.3 mm sea level rise by 2300 (Akesson et al., 2021). For all ocean forcing projections, pinning points in the bedrock geometry could halt retreat at Petermann Glacier and limit sea level rise to 3 mm even under strong ocean warming. Should the ice shelf disappear, modeling suggests that it would require ocean cooling as well as reduced calving for the ice shelf to reestablish itself over the time span of several hundred years (Akesson et al., 2022).

7. Summary

Significant progress has been made in assessing the mass balance of Petermann Ice Stream over recent decades through in-situ data collection, advances in atmospheric reanalyses, and improved ice flow modeling. However, this review identifies both knowledge gaps and data needs that remain, with the key points given below and further details in the text.

- We currently lack sufficient in-situ atmospheric monitoring (e.g. air temperatures, SMB), which is critically needed for model validation and accurate assessment of surface melting and mass balance. This concern is also applicable to many other marine-terminating glaciers in Greenland.
- There currently is no continuous monitoring of oceanographic properties within Petermann Fjord, which would help to better constrain fjord circulation models and their relationship to ice flow and atmospheric conditions.
- We lack sufficient knowledge about geology and bedrock topography beneath Petermann Glacier catchment and the interior of Greenland, which leads to uncertainties in its present basal thermal state, geothermal heat flow, and the nature of its onset region.
- Currently, subglacial runoff data is only available from modeling studies and observational data would be needed to ……

The ice–atmosphere boundary is not well-constrained at Petermann Ice Stream. While reanalyses have improved in spatial resolution over the past decades, a comparison to observational data shows that significant biases remain that can lead to incorrect estimation of surface melting. Observational data remains scarce, with no current AWS in the vicinity and no long-term, continuous data. Mass balance estimates can differ significantly depending on the ice discharge products used, with the "best estimate" mass balance shown in this review indicating an overall negative trend over the past four decades. It is apparent that there is a need for more observational data of surface climate variables to improve our understanding of ice dynamics and climate model validation.

Velocities follow a seasonal pattern of summer speed-up and winter slowdown , with large calving events, like those observed in 2008, 2010 and 2012, resulting in short-term speed-ups that are sustained over 1 to 2 years. However, if the floating tongue collapses, then the loss of backstress will result in grounding line retreat and large velocity increases inland.

Over the past decades, airborne radar flights and in-situ ocean measurements revealed large basal channels in Petermann Glacier's floating ice tongue and linked them to enhanced basal melting from atmospherically-produced subglacial runoff. The observed grounding line retreat starting in 2016 and subsequent short-term increases in ice velocity have been linked to the influx of warm AW, highlighting Petermann Ice Stream's sensitivity to ocean forcing. Additional ocean warming, in combination with increased surface melting and subglacial runoff, is anticipated to lead to the break-up of the ice tongue and further grounding line retreat as early as by 2050 . This will likely drive an inland velocity response that significantly increases ice discharge and sea level rise.

Advances have been made in determining the geological provinces beneath Petermann Ice Stream with ~80% of the catchment now being classified. However, the geology beneath the onset of Petermann Ice Stream remains unknown and boundaries between provinces are not yet well defined there. Similarly, there is currently no consensus on the origin of elevated geothermal heat flow at Petermann Ice Stream, and there could be a subglacial volcanic province in the vicinity. The basal thermal state varies significantly within the glacier's catchment, which is not well reflected in ISMIP6. Based on the well-defined shear margins and elevated basal slip ratio present at Petermann Ice Stream, we argue that Petermann Glacier should be referred to as "Ice Stream" to more accurately reflect its dynamic setting. This reclassification is significant, as ice streams can experience comparatively rapid changes in velocity and can reconfigure over the relatively short time scale of several millennia , which should be considered for model spin-up as current ice dynamics might not accurately reflect past behavior.

8. Outlook

Based on this review, we expect Petermann Ice Stream to undergo substantial dynamic changes over the next 10–20 years. Increases in air temperature will likely result in higher subglacial runoff and an earlier onset of the melt season. These changes may lead to higher basal melt rates, especially along channels in the floating tongue, which will increase thinning rates of the floating tongue thereby reducing backstress and allowing for higher flow velocities. The rifting event that initiated in 2025 will, once the ice has calved off, place Petermann Ice Stream's terminus at its most retreated position since 1923, and closer to a threshold that could result in a complete break-up of the floating tongue. We expect similar major calving events in the future, which could lead to such a break-up scenario and also induce increases in ice discharge that could result in substantial sea level rise.

Author Contributions

D.F and W.C. conceived the study. D.F. led manuscript writing and figure creation. P.W. led manuscript writing for section 2. W.C. led manuscript writing for section 4. J.A.M, P.W., A.L. and S.A.K provided feedback on the manuscript.

Acknowledgements

D.F., W.C. and S.A.K. acknowledge support from Novo Nordisk foundation grant NNF23OC00807040.

Supplementary Material

Supplementary material is available for this article and can be found here:

Petermann Review Supplementary Material

References

1. E. M. Enderlin, I. M. Howat, S. Jeong, M.-J. Noh, J. H. Angelen, M. R. Broeke, An improved mass budget for the Greenland ice sheet. *Geophys Res Lett* **41**, 866–872 (2014).
2. J. Mouginot, E. Rignot, A. A. Bjørk, M. van den Broeke, R. Millan, M. Morlighem, B. Noël, B. Scheuchl, M. Wood, Forty-six years of Greenland Ice Sheet mass balance from 1972 to 2018. *Proceedings of the National Academy of Sciences* **116**, 9239 LP – 9244 (2019).
3. I. N. Otosaka, A. Shepherd, E. R. Ivins, N.-J. Schlegel, C. Amory, M. R. van den Broeke, M. Horwath, I. Joughin, M. D. King, G. Krinner, S. Nowicki, A. J. Payne, E. Rignot, T. Scambos, K. M. Simon, B. E. Smith, L. S. Sørensen, I. Velicogna, P. L. Whitehouse, G. A, C. Agosta, A. P. Ahlstrøm, A. Blazquez, W. Colgan, M. E. Engdahl, X. Fettweis, R. Forsberg, H. Gallée, A. Gardner, L. Gilbert, N. Gourmelen, A. Groh, B. C. Gunter, C. Harig, V. Helm, S. A. Khan, C. Kittel, H. Konrad, P. L. Langen, B. S. Lecavalier, C.-C. Liang, B. D. Loomis, M. McMillan, D. Melini, S. H. Mernild, R. Mottram, J. Mouginot, J. Nilsson, B. Noël, M. E. Pattle, W. R. Peltier, N. Pie, M. Roca, I. Sasgen, H. V Save, K.-W. Seo, B. Scheuchl, E. J. O. Schrama, L. Schröder, S. B. Simonsen, T. Slater, G. Spada, T. C. Sutterley, B. D. Vishwakarma, J. M. van Wessem, D. Wiese, W. van der Wal, B. Wouters, Mass balance of the Greenland and Antarctic ice sheets from 1992 to 2020. *Earth Syst. Sci. Data* **15**, 1597–1616 (2023).
4. E. Ciracì, E. Rignot, B. Scheuchl, V. Tolpekin, M. Wollersheim, L. An, P. Milillo, J.-L. Bueso-Bello, P. Rizzoli, L. Dini, Melt rates in the kilometer-size grounding zone of Petermann Glacier, Greenland, before and during a retreat. *Proceedings of the National Academy of Sciences* **120**, e2220924120 (2023).
5. E. Rignot, P. Kanagaratnam, Changes in the velocity structure of the Greenland Ice Sheet. *Science (1979)* **311**, 986–990 (2006).
6. E. A. Hill, G. H. Gudmundsson, J. R. Carr, C. R. Stokes, Velocity response of Petermann Glacier, northwest Greenland, to past and future calving events. *Cryosphere* **12**, 3907–3921 (2018).
7. E. Bessels, *Scientific Results of the United States Arctic Expedition: Steamer Polaris, CF Hall Commanding* (US Government Printing Office, 1876)vol. 1.
8. G. S. Nares, *Narrative of a Voyage to the Polar Sea During 1875-6 in HM Ships' Alert'and'Discovery'* (London: S. Low, Marston, Searle, & Rivington, 1878)vol. 1.
9. R. Millan, J. Mouginot, A. Derkacheva, E. Rignot, P. Milillo, E. Ciraci, L. Dini, A. Bjørk, Ongoing grounding line retreat and fracturing initiated at the Petermann Glacier ice shelf, Greenland, after 2016. *Cryosphere* **16**, 3021–3031 (2022).
10. A. Münchow, L. Padman, P. Washam, K. W. Nicholls, The ice shelf of Petermann Gletscher and its connection to the Arctic and Atlantic Oceans. *Oceanography* **29**, 84–95 (2016).
11. E. Rignot, Hinge-line migration of Petermann Gletscher, north Greenland, detected using satellite-radar interferometry. *Journal of Glaciology* **44**, 469–476 (1998).

82. A. E. Hogg, A. Shepherd, N. Gourmelen, M. Engdahl, Grounding line migration from 1992 to 2011 on Petermann Glacier, North-West Greenland. *Journal of Glaciology* **62**, 1104–1114 (2016).
83. P. Washam, A. Münchow, K. W. Nicholls, A Decade of Ocean Changes Impacting the Ice Shelf of Petermann Gletscher, Greenland. *J Phys Oceanogr* **48**, 2477–2493 (2018).
84. P. Washam, K. W. Nicholls, A. Münchow, L. Padman, Summer surface melt thins Petermann Gletscher Ice Shelf by enhancing channelized basal melt. *Journal of Glaciology* **65**, 662–674 (2019).
85. R. Gadi, E. Rignot, D. Menemenlis, Modeling Ice Melt Rates From Seawater Intrusions in the Grounding Zone of Petermann Gletscher, Greenland. *Geophys Res Lett* **50**, e2023GL105869 (2023).
86. S. Ehrenfeucht, E. Rignot, M. Morlighem, Seawater Intrusion in the Observed Grounding Zone of Petermann Glacier Causes Extensive Retreat. *Geophys Res Lett* **51**, e2023GL107571 (2024).
87. S. Goliber, T. Black, TermPicks: A century of Greenland glacier terminus data for use inmachine learning applications (Version 1). Zenodo [Preprint] (2021). https://zenodo.org/records/5117931.
88. S. Goliber, T. Black, G. Catania, J. M. Lea, H. Olsen, D. Cheng, S. Bevan, A. Bjørk, C. Bunce, S. Brough, J. R. Carr, T. Cowton, A. Gardner, D. Fahrner, E. Hill, I. Joughin, N. J. Korsgaard, A. Luckman, T. Moon, T. Murray, A. Sole, M. Wood, E. Zhang, TermPicks: a century of Greenland glacier terminus data for use in scientific and machine learning applications. *Cryosphere* **16**, 3215–3233 (2022).
89. J. M. Lea, The Google Earth Engine Digitisation Tool (GEEDiT) and the Margin change Quantification Tool (MaQiT)--simple tools for the rapid mapping and quantification of changing Earth surface margins. *Earth Surface Dynamics* **6**, 551–561 (2018).
90. K. Mankoff, A. Solgaard, S. Larsen, PROMICE, I. under the E. U. H. 2020 research and innovation program, Greenland Ice Sheet solid ice discharge from 1986 through last month: Discharge. GEUS Dataverse [Preprint] (2020). https://doi.org/doi/10.22008/promice/data/ice_discharge/d/v02.
91. K. D. Mankoff, A. Solgaard, W. Colgan, A. P. Ahlstrøm, S. A. Khan, R. S. Fausto, Greenland Ice Sheet solid ice discharge from 1986 through March 2020. *Earth Syst. Sci. Data* **12**, 1367–1383 (2020).
92. W. Kochtitzky, L. Copland, M. King, R. Hugonnet, H. Jiskoot, M. Morlighem, R. Millan, S. A. Khan, B. Noël, Closing Greenland's Mass Balance: Frontal Ablation of Every Greenlandic Glacier From 2000 to 2020. *Geophys Res Lett* **50**, e2023GL104095 (2023).
93. I. Joughin, MEaSUREs Greenland Monthly Ice Sheet Velocity Mosaics from SAR and Landsat, Version 5. NASA National Snow and Ice Data Center Distributed Active Archive Center [Preprint] (2023). http://nsidc.org/data/NSIDC-0731/versions/5.
94. M. Morlighem, C. N. Williams, E. Rignot, L. An, J. E. Arndt, J. Bamber, G. Catania, N. Chauché, J. A. Dowdeswell, B. Dorschel, others, BedMachine v3: Complete bed topography and ocean bathymetry mapping of Greenland from multibeam echo sounding combined with mass conservation. *Geophys Res Lett* **44** (2017).
95. M. Morlighem, C. Williams, E. Rignot, L. An, J. E. , Arndt, J. Bamber, G. , Catania, N. Chauché, J. A. , Dowdeswell, B. Dorschel, I. Fenty, K. Hogan, I. Howat, A. Hubbard, M. Jakobsson, T. M. Jordan, K. K. Kjeldsen, R. Millan, L. Mayer, J. Mouginot, B. Noël, C. O'Cofaigh, S. J. Palmer, S.

Rysgaard, H. Seroussi, M. J. Siegert, P. Slabon, F. Straneo, M. R. van den Broeke, W. Weinrebe, M. Wood, K. Zinglersen, IceBridge BedMachine Greenland. (IDBMG4, Version 5). [Data Set]. NASA National Snow and Ice Data Center Distributed Active Archive Center. Boulder, Colorado USA. NASA National Snow and Ice Data Center Distributed Active Archive Center [Preprint] (2022). https://doi.org/https://doi.org/10.5067/GMEVBWFLWA7X.

26. B. T. Reilly, J. S. Stoner, A. C. Mix, M. H. Walczak, A. Jennings, M. Jakobsson, L. Dyke, A. Glueder, K. Nicholls, K. A. Hogan, L. A. Mayer, R. G. Hatfield, S. Albert, S. Marcott, S. Fallon, M. Cheseby, Holocene break-up and reestablishment of the Petermann Ice Tongue, Northwest Greenland. *Quat Sci Rev* **218**, 322–342 (2019).

27. M. Jakobsson, K. A. Hogan, L. A. Mayer, A. Mix, A. Jennings, J. Stoner, B. Eriksson, K. Jerram, R. Mohammad, C. Pearce, The Holocene retreat dynamics and stability of Petermann Glacier in northwest Greenland. *Nat Commun* **9**, 2104 (2018).

28. E. L. Shroyer, L. Padman, R. M. Samelson, A. Münchow, L. A. Stearns, Seasonal control of Petermann Gletscher ice-shelf melt by the ocean's response to sea-ice cover in Nares Strait. *Journal of Glaciology* **63**, 324–330 (2017).

29. K. K. Falkner, H. Melling, A. M. Münchow, J. E. Box, T. Wohlleben, H. L. Johnson, P. Gudmandsen, R. Samelson, L. Copland, K. Steffen, E. Rignot, A. K. Higgins, Context for the Recent Massive Petermann Glacier Calving Event. *Eos, Transactions American Geophysical Union* **92**, 117–118 (2011).

30. A. Münchow, L. Padman, H. A. Fricker, Interannual changes of the floating ice shelf of Petermann Gletscher, North Greenland, from 2000 to 2012. *Journal of Glaciology* **60**, 489–499 (2014).

31. F. M. Nick, A. Luckman, A. Vieli, C. J. Van Der Veen, D. Van As, R. S. W. Van De Wal, F. Pattyn, A. L. Hubbard, D. Floricioiu, The response of Petermann Glacier, Greenland, to large calving events, and its future stability in the context of atmospheric and oceanic warming. *Journal of Glaciology* **58**, 229–239 (2012).

32. A. P. Ahlstrøm, S. B. Andersen, M. L. Andersen, H. Machguth, F. M. Nick, I. Joughin, C. H. Reijmer, R. S. W. van de Wal, J. P. Merryman Boncori, J. E. Box, Seasonal velocities of eight major marine-terminating outlet glaciers of the Greenland ice sheet from continuous in situ GPS instruments. *Earth Syst Sci Data* **5**, 277–287 (2013).

33. A. J. Crawford, D. Mueller, L. Desjardins, P. G. Myers, The aftermath of Petermann Glacier calving events (2008–2012): Ice island size distributions and meltwater dispersal. *J Geophys Res Oceans* **123**, 8812–8827 (2018).

34. M. Rückamp, N. Neckel, S. Berger, A. Humbert, V. Helm, Calving induced speedup of Petermann Glacier. *J Geophys Res Earth Surf* **124**, 216–228 (2019).

35. S. Ehrenfeucht, M. Morlighem, E. Rignot, C. F. Dow, J. Mouginot, Seasonal Acceleration of Petermann Glacier, Greenland, From Changes in Subglacial Hydrology. *Geophys Res Lett* **50**, e2022GL098009 (2023).

36. E. Rignot, K. Steffen, Channelized bottom melting and stability of floating ice shelves. *Geophys Res Lett* **35** (2008).

37. E. Rignot, S. Gogineni, I. Joughin, W. Krabill, Contribution to the glaciology of northern Greenland from satellite radar interferometry. *Journal of Geophysical Research: Atmospheres* **106**, 34007–34019 (2001).

68. E. J. Rignot, S. P. Gogineni, W. B. Krabill, S. Ekholm, North and northeast Greenland ice discharge from satellite radar interferometry. *Science (1979)* **276**, 934–937 (1997).
69. E. Rignot, Tidal motion, ice velocity and melt rate of Petermann Gletscher, Greenland, measured from radar interferometry. *Journal of Glaciology* **42**, 476–485 (1996).
70. C. Heuzé, A. Wåhlin, H. L. Johnson, A. Münchow, Pathways of Meltwater Export from Petermann Glacier, Greenland. *J Phys Oceanogr* **47**, 405–418 (2017).
71. H. L. Johnson, A. Münchow, K. K. Falkner, H. Melling, Ocean circulation and properties in Petermann Fjord, Greenland. *J Geophys Res Oceans* **116** (2011).
72. D. A. Slater, F. Straneo, Submarine melting of glaciers in Greenland amplified by atmospheric warming. *Nat Geosci* **15**, 794–799 (2022).
73. H. Åkesson, M. Morlighem, M. O'Regan, M. Jakobsson, Future Projections of Petermann Glacier Under Ocean Warming Depend Strongly on Friction Law. *J Geophys Res Earth Surf* **126**, e2020JF005921 (2021).
74. J. L. Bamber, M. J. Siegert, J. A. Griggs, S. J. Marshall, G. Spada, Paleofluvial Mega-Canyon Beneath the Central Greenland Ice Sheet. *Science (1979)* **341**, 997–999 (2013).
75. R. H. Thomas, W. Abdalati, E. Frederick, W. B. Krabill, S. Manizade, K. Steffen, Investigation of surface melting and dynamic thinning on Jakobshavn Isbræ, Greenland. *Journal of Glaciology* **49**, 231–239 (2003).
76. R. J. Motyka, M. Fahnestock, M. Truffer, Volume change of Jakobshavn Isbræ, West Greenland: 1985–1997–2007. *Journal of Glaciology* **56**, 635–646 (2010).
77. E. A. Hill, G. H. Gudmundsson, J. R. Carr, C. R. Stokes, H. M. King, Twenty-first century response of Petermann Glacier, northwest Greenland to ice shelf loss. *Journal of Glaciology* **67**, 147–157 (2021).
78. A. J. Tedstone, H. Machguth, Increasing surface runoff from Greenland's firn areas. *Nat Clim Chang* **12**, 672–676 (2022).
79. C. Cai, E. Rignot, D. Menemenlis, Y. Nakayama, Observations and modeling of ocean-induced melt beneath Petermann Glacier Ice Shelf in northwestern Greenland. *Geophys Res Lett* **44**, 8396–8403 (2017).
80. W. Colgan, H. Machguth, M. MacFerrin, J. D. Colgan, D. van As, J. A. MacGregor, The abandoned ice sheet base at Camp Century, Greenland, in a warming climate. *Geophys Res Lett* **43**, 8091–8096 (2016).
81. K. Steffen, B. Vandecrux, D. Houtz, W. Abdalati, N. Bayou, J. Box, L. Colgan, L. Espona Pernas, N. Griessinger, D. Haas-Artho, GC-Net Level 1 automated weather station data. [Preprint] (2023).
82. B. Vandecrux, J. E. Box, A. P. Ahlstrøm, S. B. Andersen, N. Bayou, W. T. Colgan, N. J. Cullen, R. S. Fausto, D. Haas-Artho, A. Heilig, D. A. Houtz, P. How, I. Iosifescu Enescu, N. B. Karlsson, R. Kurup Buchholz, K. D. Mankoff, D. McGrath, N. P. Molotch, B. Perren, M. K. Revheim, A. Rutishauser, K. Sampson, M. Schneebeli, S. Starkweather, S. Steffen, J. Weber, P. J. Wright, H. J. Zwally, K. Steffen, The historical Greenland Climate Network (GC-Net) curated and augmented level-1 dataset. *Earth Syst. Sci. Data* **15**, 5467–5489 (2023).
83. J. Cappelen, Weather observations from Greenland 1958-2018. *DMI Report 19-08* (2019).
84. H. Hersbach, B. Bell, P. Berrisford, G. Biavati, A. Horányi, J. M. Sabater, J. Nicolas, C. Peubey, R. Radu, I. Rozum, ERA5 Hourly Data on Pressure Levels from 1940 to Present: Tech. Rep. doi: 10.24381/cds.bd0915c6 (2023).

55. B. Noël, W. J. van de Berg, J. M. van Wessem, E. van Meijgaard, D. van As, J. T. M. Lenaerts, S. Lhermitte, P. Kuipers Munneke, C. J. P. P. Smeets, L. H. van Ulft, R. S. W. van de Wal, M. R. van den Broeke, Modelling the climate and surface mass balance of polar ice sheets using RACMO2 – Part 1: Greenland (1958–2016). *Cryosphere* **12**, 811–831 (2018).
56. E. Dutra, J. Muñoz-Sabater, S. Boussetta, T. Komori, S. Hirahara, G. Balsamo, Environmental Lapse Rate for High-Resolution Land Surface Downscaling: An Application to ERA5. *Earth and Space Science* **7**, e2019EA000984 (2020).
57. N. Britland, "Surface Climatology and Ablation on the Floating Section of the Petermann Glacier, Greenland" (2013); https://doi.org/https://doi.org/10.5194/tc-16-4305-2022.
58. R. J. Braithwaite, Positive degree-day factors for ablation on the Greenland ice sheet studied by energy-balance modelling. *Journal of Glaciology* **41**, 153–160 (1995).
59. B. Vandecrux, J. E. Box, A. P. Ahlstrøm, S. B. Andersen, N. Bayou, W. T. Colgan, N. J. Cullen, R. S. Fausto, D. Haas-Artho, A. Heilig, D. A. Houtz, P. How, I. Iosifescu Enescu, N. B. Karlsson, R. Kurup Buchholz, K. D. Mankoff, D. McGrath, N. P. Molotch, B. Perren, M. K. Revheim, A. Rutishauser, K. Sampson, M. Schneebeli, S. Starkweather, S. Steffen, J. Weber, P. J. Wright, H. J. Zwally, K. Steffen, The historical Greenland Climate Network (GC-Net) curated and augmented level-1 dataset. *Earth Syst. Sci. Data* **15**, 5467–5489 (2023).
60. H. Machguth, H. H. Thomsen, A. Weidick, A. P. Ahlstrøm, J. Abermann, M. L. Andersen, S. B. Andersen, A. A. Bjørk, J. E. Box, R. J. Braithwaite, C. E. Bøggild, M. Citterio, P. Clement, W. Colgan, R. S. Fausto, K. Gleie, S. Gubler, B. Hasholt, B. Hynek, N. T. Knudsen, S. H. Larsen, S. H. Mernild, J. Oerlemans, H. Oerter, O. B. Olesen, C. J. P. P. Smeets, K. Steffen, M. Stober, S. Sugiyama, D. Van As, M. R. Van Den Broeke, R. S. W. Van De Wal, Greenland surface mass-balance observations from the ice-sheet ablation area and local glaciers. *Journal of Glaciology* **62**, 861–887 (2016).
61. J. H. Christensen, T. R. Carter, M. Rummukainen, G. Amanatidis, Evaluating the performance and utility of regional climate models: the PRUDENCE project. *Clim Change* **81**, 1–6 (2007).
62. R. Mottram, F. Boberg, P. L. Langen, S. Yang, C. Rodehacke, J. H. Christensen, M. S. Madsen, Surface mass balance of the Greenland ice sheet in the regional climate model HIRHAM5: Present state and future prospects. *Low Temperature Science* **75**, 105–115 (2017).
63. M. Tedesco, X. Fettweis, Unprecedented atmospheric conditions (1948–2019) drive the 2019 exceptional melting season over the Greenland ice sheet. *Cryosphere* **14**, 1209–1223 (2020).
64. J. Mouginot, E. Rignot, Glacier catchments/basins for the Greenland Ice Sheet [Dataset]. Dryad [Preprint] (2019). https://doi.org/10.7280/D1WT11.
65. Q. Glaude, B. Noel, M. Olesen, M. Van den Broeke, W. J. van de Berg, R. Mottram, N. Hansen, A. Delhasse, C. Amory, C. Kittel, H. Goelzer, X. Fettweis, A Factor Two Difference in 21st-Century Greenland Ice Sheet Surface Mass Balance Projections From Three Regional Climate Models Under a Strong Warming Scenario (SSP5-8.5). *Geophys Res Lett* **51**, e2024GL111902 (2024).
66. X. Fettweis, S. Hofer, U. Krebs-Kanzow, C. Amory, T. Aoki, C. J. Berends, A. Born, J. E. Box, A. Delhasse, K. Fujita, P. Gierz, H. Goelzer, E. Hanna, A. Hashimoto, P. Huybrechts, M.-L. Kapsch, M. D. King, C. Kittel, C. Lang, P. L. Langen, J. T. M. Lenaerts, G. E. Liston, G. Lohmann, S. H. Mernild, U. Mikolajewicz, K. Modali, R. H. Mottram, M. Niwano, B. Noël, J. C. Ryan, A. Smith, J. Streffing, M. Tedesco, W. J. van de Berg, M. van den Broeke, R. S. W. van de Wal, L. van Kampenhout, D. Wilton, B. Wouters, F. Ziemen, T. Zolles, GrSMBMIP:

intercomparison of the modelled 1980–2012 surface mass balance over the Greenland Ice Sheet. *Cryosphere* **14**, 3935–3958 (2020).
67. I. Joughin, B. E. Smith, I. M. Howat, T. Scambos, T. Moon, Greenland flow variability from ice-sheet-wide velocity mapping. *Journal of Glaciology* **56**, 415–430 (2010).
68. I. Joughin, B. E. Smith, I. Howat, Greenland Ice Mapping Project: ice flow velocity variation at sub-monthly to decadal timescales. *Cryosphere* **12**, 2211–2227 (2018).
69. A. Solgaard, A. Kusk, Greenland Ice Velocity from Sentinel-1 Edition 3. [Preprint] (2021).
70. A. Solgaard, A. Kusk, J. P. Merryman Boncori, J. Dall, K. D. Mankoff, A. P. Ahlstrøm, S. B. Andersen, M. Citterio, N. B. Karlsson, K. K. Kjeldsen, N. J. Korsgaard, S. H. Larsen, R. S. Fausto, Greenland ice velocity maps from the PROMICE project. *Earth Syst. Sci. Data* **13**, 3491–3512 (2021).
71. A. S. Gardner, M. A. Fahnestock, T. A. Scambos, ITS_LIVE Regional Glacier and Ice Sheet Surface Velocities, National Snow and Ice Data Center. [Preprint] (2019).
72. A. S. Gardner, G. Moholdt, T. Scambos, M. Fahnstock, S. Ligtenberg, M. van den Broeke, J. Nilsson, Increased West Antarctic and unchanged East Antarctic ice discharge over the last 7 years. *Cryosphere* **12**, 521–547 (2018).
73. E. A. Hill, J. R. Carr, C. R. Stokes, G. H. Gudmundsson, Dynamic changes in outlet glaciers in northern Greenland from 1948 to 2015. *Cryosphere* **12**, 3243–3263 (2018).
74. N. Wilson, F. Straneo, P. Heimbach, Satellite-derived submarine melt rates and mass balance (2011–2015) for Greenland's largest remaining ice tongues. *Cryosphere* **11**, 2773–2782 (2017).
75. M. G. Wearing, L. A. Stevens, P. Dutrieux, J. Kingslake, Ice-Shelf Basal Melt Channels Stabilized by Secondary Flow. *Geophys Res Lett* **48**, e2021GL094872 (2021).
76. C. F. Dow, W. S. Lee, J. S. Greenbaum, C. A. Greene, D. D. Blankenship, K. Poinar, A. L. Forrest, D. A. Young, C. J. Zappa, Basal channels drive active surface hydrology and transverse ice shelf fracture. *Sci Adv* **4**, eaao7212 (2018).
77. A. Münchow, Volume and Freshwater Flux Observations from Nares Strait to the West of Greenland at Daily Time Scales from 2003 to 2009. *J Phys Oceanogr* **46**, 141–157 (2016).
78. A. Münchow, K. K. Falkner, H. Melling, B. Rabe, H. L. Johnson, Ocean warming of Nares Strait bottom waters. *Oceanography* **24**, 114 (2011).
79. A. Münchow, K. K. Falkner, H. Melling, Baffin Island and West Greenland Current Systems in northern Baffin Bay. *Prog Oceanogr* **132**, 305–317 (2015).
80. J. Huang, R. S. Pickart, F. Bahr, L. T. McRaven, J.-É. Tremblay, C. Michel, E. Jeansson, B. Kopec, J. M. Welker, S. R. Ólafsdóttir, Water mass evolution and general circulation of Baffin Bay: Observations from two shipboard surveys in 2021. *Prog Oceanogr* **229**, 103322 (2024).
81. L. de Steur, M. Steele, E. Hansen, J. Morison, I. Polyakov, S. M. Olsen, H. Melling, F. A. McLaughlin, R. Kwok, W. M. Smethie Jr., P. Schlosser, Hydrographic changes in the Lincoln Sea in the Arctic Ocean with focus on an upper ocean freshwater anomaly between 2007 and 2010. *J Geophys Res Oceans* **118**, 4699–4715 (2013).
82. S. S. Jacobs, A. Jenkins, C. F. Giulivi, P. Dutrieux, Stronger ocean circulation and increased melting under Pine Island Glacier ice shelf. *Nat Geosci* **4**, 519–523 (2011).
83. P. Washam, K. W. Nicholls, A. Münchow, L. Padman, Tidal Modulation of Buoyant Flow and Basal Melt Beneath Petermann Gletscher Ice Shelf, Greenland. *J Geophys Res Oceans* **125**, e2020JC016427 (2020).

84. E. Rignot, N. Chauche, R. Gadi, S. Ehrenfeucht, E. Ciraci, Grounding Line Remote Operated Vehicle (GROV) Survey of the Ice Shelf Cavity of Petermann Glacier, Greenland. *Geophys Res Lett* **52**, e2024GL113400 (2025).
85. A. Prakash, Q. Zhou, T. Hattermann, N. Kirchner, Enhanced subglacial discharge amplifies Petermann Ice Shelf melting when ocean thermal forcing saturates. *Nat Commun* **16**, 4213 (2025).
86. P. Dutrieux, C. Stewart, A. Jenkins, K. W. Nicholls, H. F. J. Corr, E. Rignot, K. Steffen, Basal terraces on melting ice shelves. *Geophys Res Lett* **41**, 5506–5513 (2014).
87. B. E. Schmidt, P. Washam, P. E. D. Davis, K. W. Nicholls, D. M. Holland, J. D. Lawrence, K. L. Riverman, J. A. Smith, A. Spears, D. J. G. Dichek, A. D. Mullen, E. Clyne, B. Yeager, P. Anker, M. R. Meister, B. C. Hurwitz, E. S. Quartini, F. E. Bryson, A. Basinski-Ferris, C. Thomas, J. Wake, D. G. Vaughan, S. Anandakrishnan, E. Rignot, J. Paden, K. Makinson, Heterogeneous melting near the Thwaites Glacier grounding line. *Nature* **614**, 471–478 (2023).
88. D. M. Holland, R. H. Thomas, B. de Young, M. H. Ribergaard, B. Lyberth, Acceleration of Jakobshavn Isbræ triggered by warm subsurface ocean waters. *Nat Geosci* **1**, 659–664 (2008).
89. H. Åkesson, M. Morlighem, J. Nilsson, C. Stranne, M. Jakobsson, Petermann ice shelf may not recover after a future breakup. *Nat Commun* **13**, 2519 (2022).
90. O. M. Johannessen, B. Mohamed, M. W. and Miles, Unprecedented Retreat in a 50-Year Observational Record for Petermann Glacier, North Greenland. *Atmospheric and Oceanic Science Letters* **6**, 259–265 (2013).
91. M. R. England, I. Eisenman, N. J. Lutsko, T. J. W. Wagner, The recent emergence of Arctic Amplification. *Geophys Res Lett*, e2021GL094086 (2021).
92. B. Noël, W. J. van de Berg, S. Lhermitte, M. R. van den Broeke, Rapid ablation zone expansion amplifies north Greenland mass loss. *Sci Adv* **5**, eaaw0123 (2025).
93. M. C. Serreze, A. P. Barrett, J. C. Stroeve, D. N. Kindig, M. M. Holland, The emergence of surface-based Arctic amplification. *Cryosphere* **3**, 11–19 (2009).
94. P. R. Dawes, The bedrock geology under the Inland Ice: the next major challenge for Greenland mapping. *GEUS Bulletin* **17**, 57–60 (2009).
95. J. A. MacGregor, W. T. Colgan, G. J. G. Paxman, K. J. Tinto, B. Csathó, F. A. Darbyshire, M. A. Fahnestock, T. F. Kokfelt, E. J. MacKie, M. Morlighem, O. V Sergienko, Geologic Provinces Beneath the Greenland Ice Sheet Constrained by Geophysical Data Synthesis. *Geophys Res Lett* **51**, e2023GL107357 (2024).
96. I. Howat, MEaSUREs Greenland Ice Mapping Project (GIMP) Land Ice and Ocean Classification Mask. . NASA National Snow and Ice Data Center Distributed Active Archive Center.[describe subset used if applicable]. Date Accessed 04-25-2025. (NSIDC-0714, Version 1) [Preprint] (2017). https://doi.org/https://doi.org/10.5067/B8X58MQBFUPA.
97. J. A. MacGregor, W. Chu, W. T. Colgan, M. A. Fahnestock, D. Felikson, N. B. Karlsson, S. M. J. Nowicki, M. Studinger, GBaTSv2: a revised synthesis of the likely basal thermal state of the Greenland Ice Sheet. *Cryosphere* **16**, 3033–3049 (2022).
98. K. J. Tinto, R. E. Bell, J. R. Cochran, A. Münchow, Bathymetry in Petermann fjord from Operation IceBridge aerogravity. *Earth Planet Sci Lett* **422**, 58–66 (2015).
99. Y. M. Martos, T. A. Jordan, M. Catalán, T. M. Jordan, J. L. Bamber, D. G. Vaughan, Geothermal Heat Flux Reveals the Iceland Hotspot Track Underneath Greenland. *Geophys Res Lett* **45**, 8214–8222 (2018).

100. W. Colgan, A. Wansing, K. Mankoff, M. Lösing, J. Hopper, K. Louden, J. Ebbing, F. G. Christiansen, T. Ingeman-Nielsen, L. C. Liljedahl, J. A. MacGregor, Á. Hjartarson, S. Bernstein, N. B. Karlsson, S. Fuchs, J. Hartikainen, J. Liakka, R. S. Fausto, D. Dahl-Jensen, A. Bjørk, J.-O. Naslund, F. Mørk, Y. Martos, N. Balling, T. Funck, K. K. Kjeldsen, D. Petersen, U. Gregersen, G. Dam, T. Nielsen, S. A. Khan, A. Løkkegaard, Greenland Geothermal Heat Flow Database and Map (Version 1). *Earth Syst. Sci. Data* **14**, 2209–2238 (2022).
101. P. R. Dawes, B. Thomassen, T. I. H. Andersson, A new volcanic province: evidence from glacial erratics in western North Greenland. *Geology of Greenland Survey Bulletin* **186**, 35–41 (2000).
102. M. Truffer, K. A. Echelmeyer, Of isbræ and ice streams. *Ann Glaciol* **36**, 66–72 (2003).
103. M. A. Cooper, T. M. Jordan, D. M. Schroeder, M. J. Siegert, C. N. Williams, J. L. Bamber, Subglacial roughness of the Greenland Ice Sheet: relationship with contemporary ice velocity and geology. *Cryosphere* **13**, 3093–3115 (2019).
104. M. A. Cooper, T. M. Jordan, M. J. Siegert, J. L. Bamber, Surface Expression of Basal and Englacial Features, Properties, and Processes of the Greenland Ice Sheet. *Geophys Res Lett* **46**, 783–793 (2019).
105. C. Hulbe, M. Fahnestock, Century-scale discharge stagnation and reactivation of the Ross ice streams, West Antarctica. *J Geophys Res Earth Surf* **112** (2007).
106. D. Jansen, S. Franke, C. C. Bauer, T. Binder, D. Dahl-Jensen, J. Eichler, O. Eisen, Y. Hu, J. Kerch, M.-G. Llorens, H. Miller, N. Neckel, J. Paden, T. de Riese, T. Sachau, N. Stoll, I. Weikusat, F. Wilhelms, Y. Zhang, P. D. Bons, Shear margins in upper half of Northeast Greenland Ice Stream were established two millennia ago. *Nat Commun* **15**, 1193 (2024).
107. S. Franke, P. D. Bons, J. Westhoff, I. Weikusat, T. Binder, K. Streng, D. Steinhage, V. Helm, O. Eisen, J. D. Paden, G. Eagles, D. Jansen, Holocene ice-stream shutdown and drainage basin reconfiguration in northeast Greenland. *Nat Geosci* **15**, 995–1001 (2022).
108. A. Aschwanden, D. J. Brinkerhoff, Calibrated Mass Loss Predictions for the Greenland Ice Sheet. *Geophys Res Lett* **49**, e2022GL099058 (2022).
109. I. Joughin, B. Smith, I. Howat, T. Scambos, MEaSUREs Multi-year Greenland Ice Sheet Velocity Mosaic (NSIDC-0670,Version 1). NASA National Snow and Ice Data Center Distributed Active Archive Center [Preprint] (2016). https://doi.org/https://doi.org/10.5067/QUA5Q9SVMSJG.
110. I. Joughin, B. E. Smith, I. M. Howat, A complete map of Greenland ice velocity derived from satellite data collected over 20 years. *Journal of Glaciology* **64**, 1–11 (2018).
111. D. Felikson, T. C. Bartholomaus, G. A. Catania, N. J. Korsgaard, K. H. Kjær, M. Morlighem, B. Noël, M. Van Den Broeke, L. A. Stearns, E. L. Shroyer, others, Inland thinning on the Greenland ice sheet controlled by outlet glacier geometry. *Nat Geosci* **10**, 366 (2017).
112. D. Felikson, G. Catania, T. C. Bartholomaus, M. Morlighem, B. P. Y. Noël, Steep glacier bed knickpoints mitigate inland thinning in Greenland. *Geophys Res Lett* **48**, e2020GL090112 (2021).
113. E. Carnahan, G. Catania, T. C. Bartholomaus, Observed mechanism for sustained glacier retreat and acceleration in response to ocean warming around Greenland. *Cryosphere* **16**, 4305–4317 (2022).
114. S. F. Price, A. J. Payne, I. M. Howat, B. E. Smith, Committed sea-level rise for the next century from Greenland ice sheet dynamics during the past decade. *Proceedings of the National Academy of Sciences* **108**, 8978–8983 (2011).

115. G. J. G. Paxman, K. J. Tinto, J. Austermann, Neogene-Quaternary Uplift and Landscape Evolution in Northern Greenland Recorded by Subglacial Valley Morphology. *J Geophys Res Earth Surf* **126**, e2021JF006395 (2021).
116. B. A. Kiesling, L. T. Nielsen, C. S. Hvidberg, R. Nuterman, R. M. DeConto, Pliocene–Pleistocene megafloods as a mechanism for Greenlandic megacanyon formation. *Geology* **48**, 737–741 (2020).
117. G. Dam, M. Sønderholm, E. V. Sørensen, Pliocene–Pleistocene megafloods as a mechanism for Greenlandic megacanyon formation: COMMENT. *Geology* **48**, e511–e511 (2020).
118. J. S. Bowling, S. J. Livingstone, A. J. Sole, W. Chu, Distribution and dynamics of Greenland subglacial lakes. *Nat Commun* **10**, 2810 (2019).
119. J. A. MacGregor, L. N. Boisvert, B. Medley, A. A. Petty, J. P. Harbeck, R. E. Bell, J. B. Blair, E. Blanchard-Wrigglesworth, E. M. Buckley, M. S. Christoffersen, J. R. Cochran, B. M. Csathó, E. L. De Marco, R. T. Dominguez, M. A. Fahnestock, S. L. Farrell, S. P. Gogineni, J. S. Greenbaum, C. M. Hansen, M. A. Hofton, J. W. Holt, K. C. Jezek, L. S. Koenig, N. T. Kurtz, R. Kwok, C. F. Larsen, C. J. Leuschen, C. D. Locke, S. S. Manizade, S. Martin, T. A. Neumann, S. M. J. Nowicki, J. D. Paden, J. A. Richter-Menge, E. J. Rignot, F. Rodríguez-Morales, M. R. Siegfried, B. E. Smith, J. G. Sonntag, M. Studinger, K. J. Tinto, M. Truffer, T. P. Wagner, J. E. Woods, D. A. Young, J. K. Yungel, The Scientific Legacy of NASA's Operation IceBridge. *Reviews of Geophysics* **59**, e2020RG000712 (2021).
120. W. Chu, D. M. Schroeder, H. Seroussi, T. T. Creyts, R. E. Bell, Complex Basal Thermal Transition Near the Onset of Petermann Glacier, Greenland. *J Geophys Res Earth Surf* **123**, 985–995 (2018).
121. P. D. Bons, D. Jansen, F. Mundel, C. C. Bauer, T. Binder, O. Eisen, M. W. Jessell, M.-G. Llorens, F. Steinbach, D. Steinhage, I. Weikusat, Converging flow and anisotropy cause large-scale folding in Greenland's ice sheet. *Nat Commun* **7**, 11427 (2016).
122. R. E. Bell, K. Tinto, I. Das, M. Wolovick, W. Chu, T. T. Creyts, N. Frearson, A. Abdi, J. D. Paden, Deformation, warming and softening of Greenland's ice by refreezing meltwater. *Nat Geosci* **7**, 497–502 (2014).
123. G. J.-M. C. Leysinger Vieli, C. Martín, R. C. A. Hindmarsh, M. P. Lüthi, Basal freeze-on generates complex ice-sheet stratigraphy. *Nat Commun* **9**, 4669 (2018).
124. J. A. MacGregor, M. A. Fahnestock, W. T. Colgan, N. K. Larsen, K. K. Kjeldsen, J. M. Welker, The age of surface-exposed ice along the northern margin of the Greenland Ice Sheet. *Journal of Glaciology* **66**, 667–684 (2020).

Supplementary Material

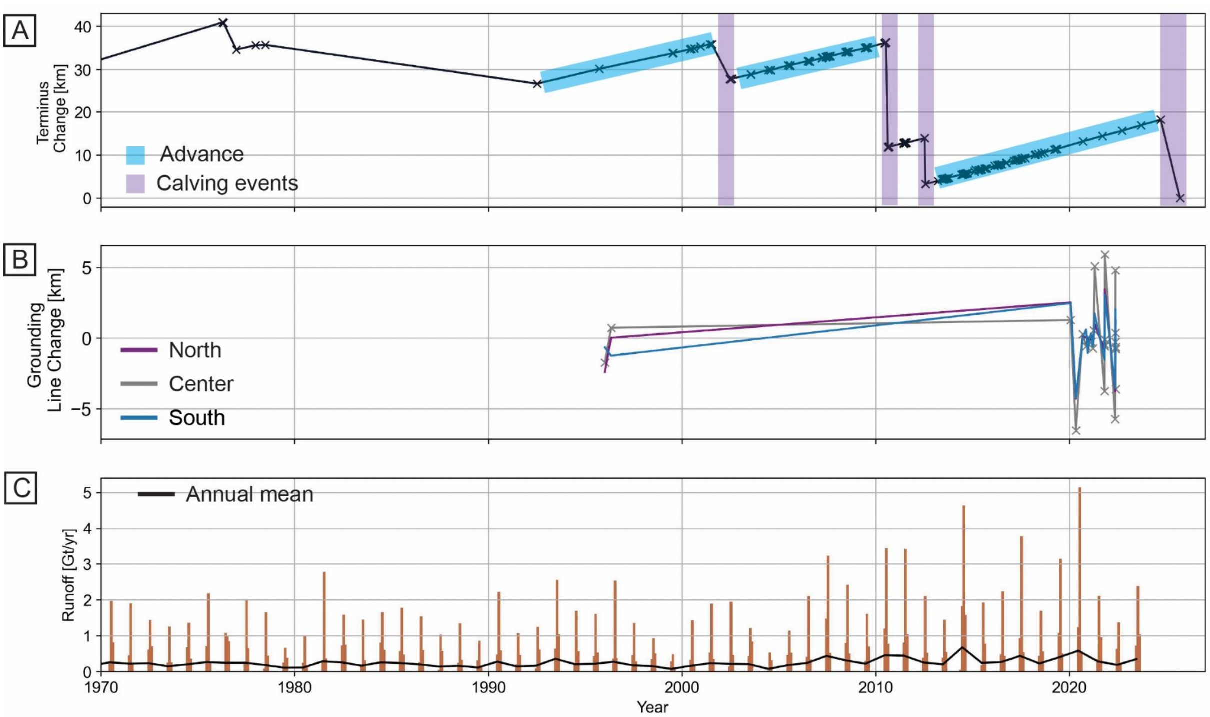

Figure S1 | Terminus and grounding zone change, and subglacial runoff at Petermann Glacier
A) *Terminus position change along the centerline from TermPicks dataset (10, 11) extended to present day using GEEDiT (calculated using MAQiT) (12). Shaded areas mark large calving events (purple) and periods of advance (blue).* ***B)*** *Grounding Line change along the centerline (13).* ***C)*** *Runoff extracted from monthly MAR3.14 (14) reanalysis data as weighted catchment average with annual mean shown in black.*

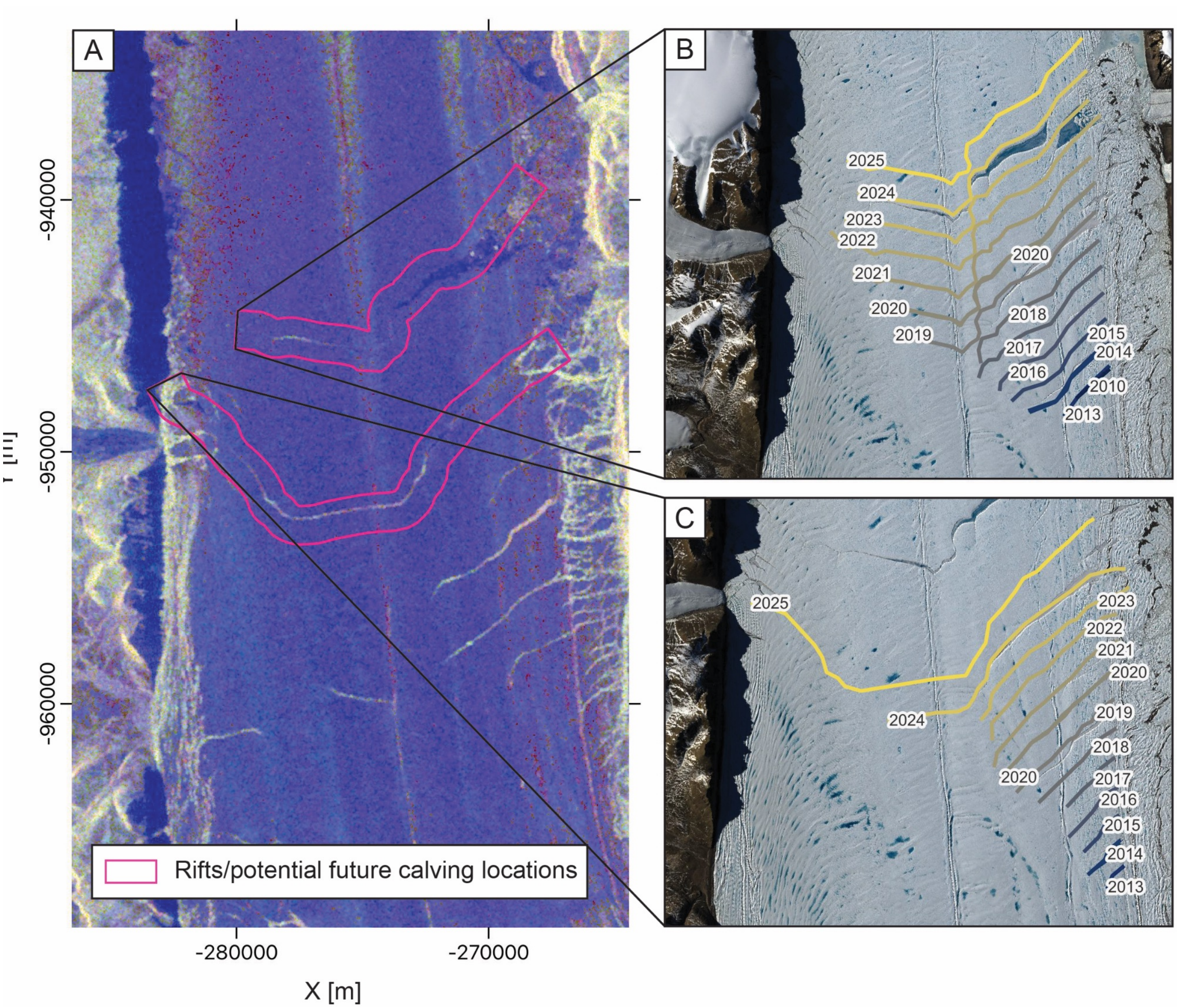

Figure S2 | Sentinel-1 image of ongoing calving event
A) Stacked Sentinel 1 image (Band1: HH, Band2: HV, Band3: HH): from 19/03/2026 showing two large rifts near the terminus of Petermann Glacier at a distance of ~12.8 and 19 km from the terminus. The rift at 19 km from the

terminus appears to have reached the full width of the glacier indicating that a calving event is currently underway. B) evolution of the rift at ~12.8 km from the terminus delineated using GEEDiT (Lea, 2018) on top of a pansharpened Landsat 8 image from 17/06/2024. C) Same as in B) for the rift at ~19 km from the terminus.

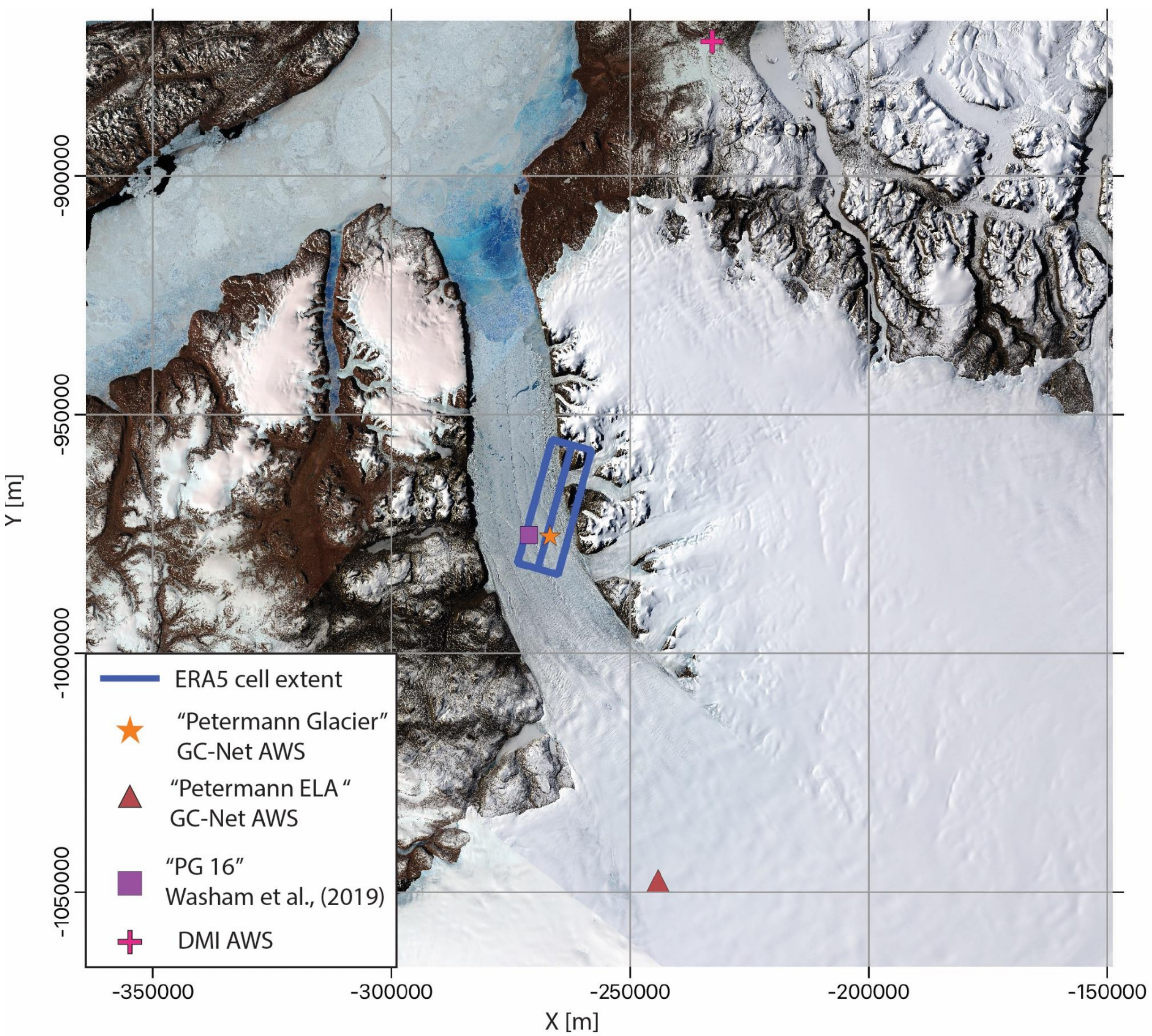

Figure S3 | Petermann weather station overview

Location of ERA5 (1) grid cell, DMI automatic weather station (AWS) in Hall Land (pink cross), GC-Net "Petermann ELA" AWS (red triangle) and "GC-Net "Petermann Glacier" AWS (yellow star) (2, 3), MAR 3.14 grid point (green circle), and PG16 weather station established by the University of Delaware (4) Basemap is a pan-sharpened Landsat-8/9 Mosaic from 17/06/2024. Note: Grid cells are equilateral but are distorted due to the Polar Stereographic coordinate system. The X and Y axis are polar stereographic coordinates (EPSG: 3413).

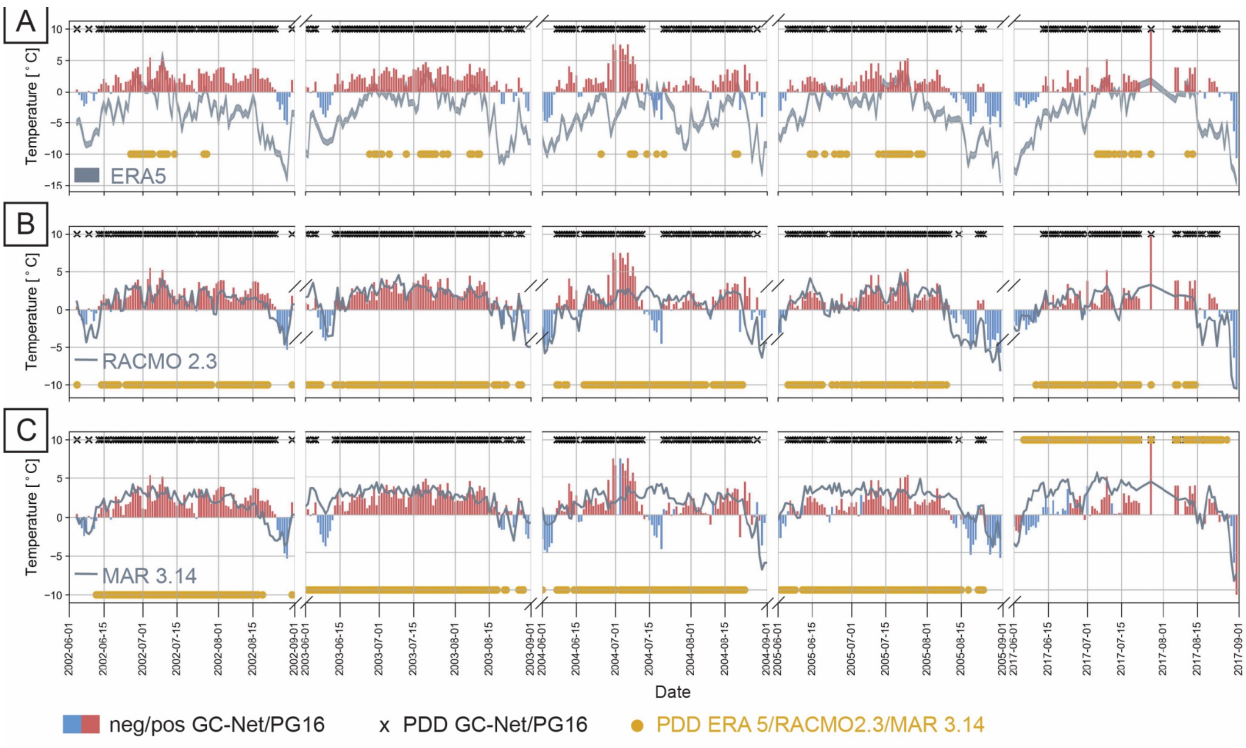

Figure S4* | *Positive Degree Day overview

Positive degree days for A) ERA5, GC-Net and PG16, with positive degree days for observational data shown as black x and for reanalysis data as yellow o. B) same as A) but for RACMO2.3 reanalysis data. C) same as in A) but for MAR 3.14 reanalysis data.

Table S1* | *Overview of solid ice discharge datasets

Overview of solid ice discharge datasets with differences in flux gate locations, velocity products, surface elevation, bedrock topography and temporal resolutions (*5*–*9*).

Author	Flux gate distance to 2017 grounding zone	Velocity produts used	Surface elevation	bedrock topography	Temporal resolution
Kochtitzky et al., 2023	~ 5 kilometres	MEaSUREs version 2 (Joughin et al., 2018) ITS_LIVE (Gardner et al., 2019)	Operation Ice Bridge observations (MacGregor et al., 2021) BedMachine version 4 (Morlighem et al., 2017)	BedMachine version 4 (Morlighem et al., 2017)	Decadal
Mankoff et al., 2020	~ 9 kilometers	Sentinel 1 MEaSUREs version 2 (Joughin et al, 2018) MEaSUREs version 2 (Howat et al., 2017)	GIMP DEM (Howat et al., 2014) Surface elevation change rates (Khan, 2017)	BedMachine version 3 (Morlighem et al., 2017)	Monthly
Mouginot et al., 2019	Within 1km of the most retreated grounding line position	Multiple sources (see Mouginot et al., (2019) appendix Table S1)	AeroDEM (Korsgaard et al., 2016) LiDAR ATM (Krabill et al., 2000, Krabill 2010) IceSAT (Zwally et al., 2014) GIMP DEM (Howat et al., 2014) ArcticDEM (Porter et al., 2018)	Direct radar sounder measurements (Gogineni et al., 2001) BedMachine version 3 (Morlighem et al., 2017)	Annually

Table S2 | Decadal mean ice discharge comparison

Comparison of decadal means for each ice discharge data product with change to previous period shown in parenthesis (5–9).

Dataset	Mean ice discharge 1990–2000 [Gt/yr]	Mean ice discharge 2000–2010 [Gt/yr]	Mean ice discharge 2010–2017 [Gt/yr]	Change between 1990-2000 and 2010-2017
Mouginot et al., 2019	10.7	10.6 (-1 %)	11.4 (+7 %)	+ 6 %
Mankoff et al., 2020	12.1	11.4 (-6 %)	11.6 (+2 %)	-4%
Kochtitzky et al., 2023	N/A	10.32	10.42 (+1 %)	+ 1 %

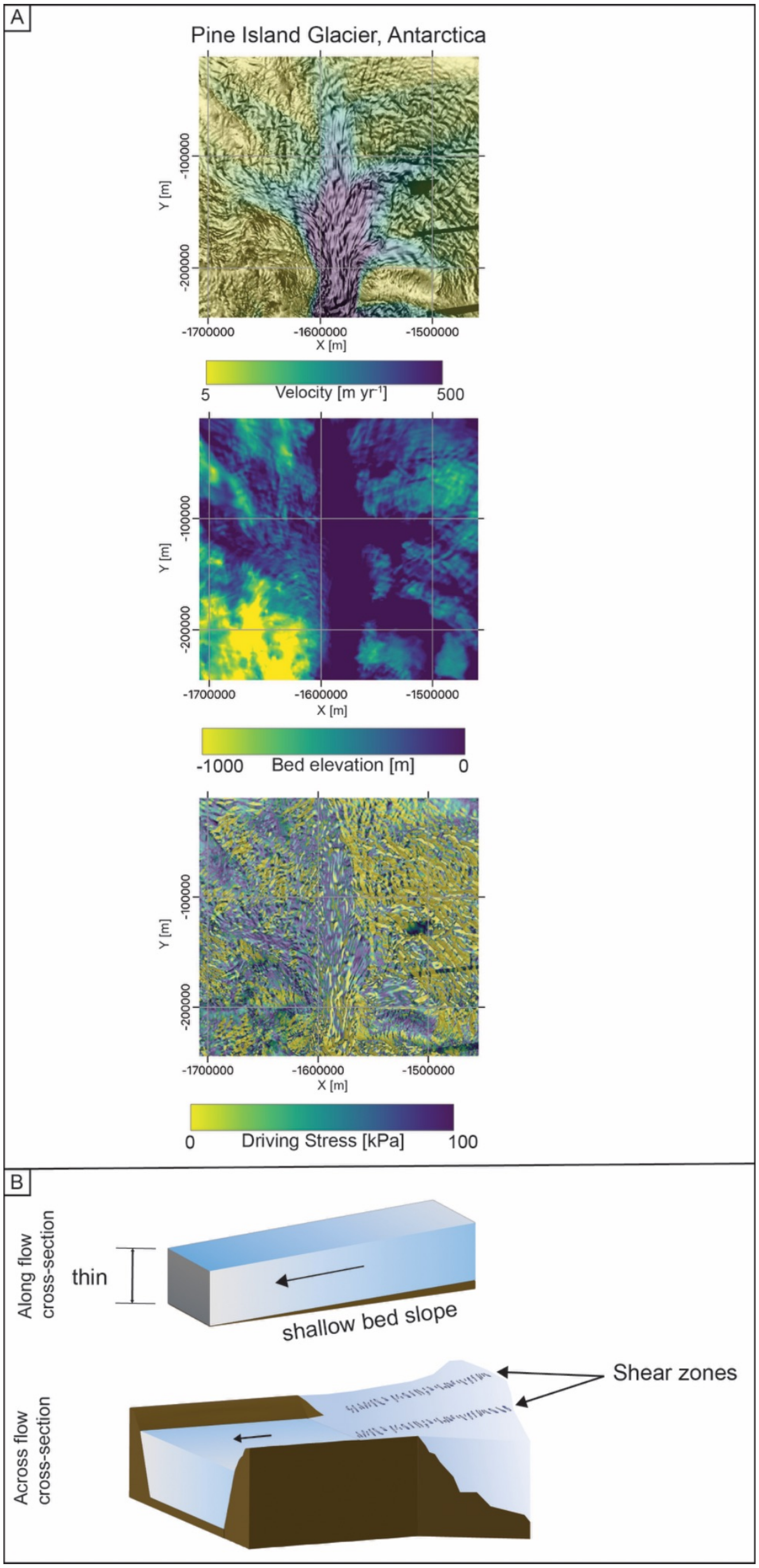

Figure S5 | Onset of Pine Island Glacier Antarctica
Flow-aware hillshade from REMA that mostly highlights the surface expression of basal topographic relief (*95*) *overlaid with a MEaSUREs multi-year velocity mosaic* (Rignot et al., 2011; Mouginot et al., 2012; Rignot et al., 2017; Mouginot

et al., 2017;) *bedrock topography from BedMachine Antarctica v4* (Morlighem et al., 2020; Morlighem 2026) *and driving stress calculated from BedMachine v4 and MEaSUREs multi-year velocity mosaic for Pine Island Glacier, Antarctica* ***B)*** *Conceptual sketch for along flow and across flow cross sections for Ice Streams. The X and Y axis represents Antarctic polar stereographic coordinates (EPSG: 3031).*

References

1. H. Hersbach, B. Bell, P. Berrisford, G. Biavati, A. Horányi, J. M. Sabater, J. Nicolas, C. Peubey, R. Radu, I. Rozum, ERA5 Hourly Data on Pressure Levels from 1940 to Present: Tech. Rep. doi: 10.24381/cds.bd0915c6 (2023).
2. K. Steffen, B. Vandecrux, D. Houtz, W. Abdalati, N. Bayou, J. Box, L. Colgan, L. Espona Pernas, N. Griessinger, D. Haas-Artho, GC-Net Level 1 automated weather station data. [Preprint] (2023).
3. B. Vandecrux, J. E. Box, A. P. Ahlstrøm, S. B. Andersen, N. Bayou, W. T. Colgan, N. J. Cullen, R. S. Fausto, D. Haas-Artho, A. Heilig, D. A. Houtz, P. How, I. Iosifescu Enescu, N. B. Karlsson, R. Kurup Buchholz, K. D. Mankoff, D. McGrath, N. P. Molotch, B. Perren, M. K. Revheim, A. Rutishauser, K. Sampson, M. Schneebeli, S. Starkweather, S. Steffen, J. Weber, P. J. Wright, H. J. Zwally, K. Steffen, The historical Greenland Climate Network (GC-Net) curated and augmented level-1 dataset. *Earth Syst. Sci. Data* **15**, 5467–5489 (2023).
4. P. Washam, K. W. Nicholls, A. Münchow, L. Padman, Summer surface melt thins Petermann Gletscher Ice Shelf by enhancing channelized basal melt. *Journal of Glaciology* **65**, 662–674 (2019).
5. K. D. Mankoff, A. Solgaard, W. Colgan, A. P. Ahlstrøm, S. A. Khan, R. S. Fausto, Greenland Ice Sheet solid ice discharge from 1986 through March 2020. *Earth Syst. Sci. Data* **12**, 1367–1383 (2020).
6. K. Mankoff, A. Solgaard, S. Larsen, PROMICE, I. under the E. U. H. 2020 research and innovation program, Greenland Ice Sheet solid ice discharge from 1986 through last month: Discharge. GEUS Dataverse [Preprint] (2020). https://doi.org/doi/10.22008/promice/data/ice_discharge/d/v02.
7. W. Kochtitzky, L. Copland, M. King, R. Hugonnet, H. Jiskoot, M. Morlighem, R. Millan, S. A. Khan, B. Noël, Closing Greenland's Mass Balance: Frontal Ablation of Every Greenlandic Glacier From 2000 to 2020. *Geophys Res Lett* **50**, e2023GL104095 (2023).
8. J. Mouginot, E. Rignot, A. A. Bjørk, M. van den Broeke, R. Millan, M. Morlighem, B. Noël, B. Scheuchl, M. Wood, Forty-six years of Greenland Ice Sheet mass balance from 1972 to 2018. *Proceedings of the National Academy of Sciences* **116**, 9239 LP – 9244 (2019).

9. B. Noël, W. J. van de Berg, J. M. van Wessem, E. van Meijgaard, D. van As, J. T. M. Lenaerts, S. Lhermitte, P. Kuipers Munneke, C. J. P. P. Smeets, L. H. van Ulft, R. S. W. van de Wal, M. R. van den Broeke, Modelling the climate and surface mass balance of polar ice sheets using RACMO2 – Part 1: Greenland (1958–2016). *Cryosphere* **12**, 811–831 (2018).
10. S. Goliber, T. Black, TermPicks: A century of Greenland glacier terminus data for use inmachine learning applications (Version 1). Zenodo [Preprint] (2021). https://zenodo.org/records/5117931.
11. S. Goliber, T. Black, G. Catania, J. M. Lea, H. Olsen, D. Cheng, S. Bevan, A. Bjørk, C. Bunce, S. Brough, J. R. Carr, T. Cowton, A. Gardner, D. Fahrner, E. Hill, I. Joughin, N. J. Korsgaard, A. Luckman, T. Moon, T. Murray, A. Sole, M. Wood, E. Zhang, TermPicks: a century of Greenland glacier terminus data for use in scientific and machine learning applications. *Cryosphere* **16**, 3215–3233 (2022).
12. J. M. Lea, The Google Earth Engine Digitisation Tool (GEEDiT) and the Margin change Quantification Tool (MaQiT)--simple tools for the rapid mapping and quantification of changing Earth surface margins. *Earth Surface Dynamics* **6**, 551–561 (2018).
13. E. Ciracì, E. Rignot, B. Scheuchl, V. Tolpekin, M. Wollersheim, L. An, P. Milillo, J.-L. Bueso-Bello, P. Rizzoli, L. Dini, Melt rates in the kilometer-size grounding zone of Petermann Glacier, Greenland, before and during a retreat. *Proceedings of the National Academy of Sciences* **120**, e2220924120 (2023).
14. M. Tedesco, X. Fettweis, Unprecedented atmospheric conditions (1948–2019) drive the 2019 exceptional melting season over the Greenland ice sheet. *Cryosphere* **14**, 1209–1223 (2020).